the mRNA expression for 35 of 47 genes linked to energy production and redox regulation, 11 of 16 energy metabolism-related genes, and five of six cholesterol metabolism-related genes was significantly suppressed at one or more time points. However, there was no significant difference in the hepatic mRNA expression levels of clock genes between the mice fed the atherogenic diet and control mice at any time point (Supplemental Table 2). This finding was verified by real-time quantitative PCR (Fig. 1).

In control mice, the DNA chip analyses detected rhythmic mRNA expression in 31 genes, in addition to the clock genes (Fig. 2, Supplemental Fig. 4 and Supplemental Table 1). As reported previously [16], daily expression profiles of *Cyp7a1* gene were opposite in phase between the groups (Fig. 2D). Additionally, the atherogenic diet dampened the mRNA expression rhythms in two of two genes related to ROS defense and seven of eight genes involved in protein degradation (Fig. 2E, Supplemental Fig. 4A and Supplemental Table 1). However, transcript levels of most of the genes related to energy production, redox regulation, MAPK cascade, nuclear receptors, and energy and cholesterol metabolism, as well as the clock genes, showed significant 24-h rhythmicity in mice fed the atherogenic diet and in control mice (Fig. 2A–D, Supplemental Fig. 4B and Supplemental Table 1). These results suggest that the circadian clock function is maintained in the livers of mice with NASH, probably due to compensating alterations in the expression of various genes, including ROS defense- and protein degradation-associated genes.

Discussion

Accumulating evidence shows that the circadian clock regulates many physiological functions, such as carbohydrate and lipid metabolism [4], mitochondrial energy production, redox regulation, ROS defense [30,31], and MAPK activity [32]. Thus, it is not surprising that dysfunction in the circadian clock can cause various disorders, including metabolic syndrome [5] and malignancies [33]. However, whether these pathological conditions *per se* cause impairment of clock function remains to be clarified. In particular, our previous finding [16] that simple fatty liver induced by high-fat feeding had little effect on the hepatic circadian clock in mice differs considerably from the results of Kohsaka et al. [13]. To address this issue, we developed a severe NASH model, with oxidative stress and drastic metabolic changes, and investigated the expression rhythms of the clock genes and metabolism- and inflammation-associated genes in the liver of this animal model.
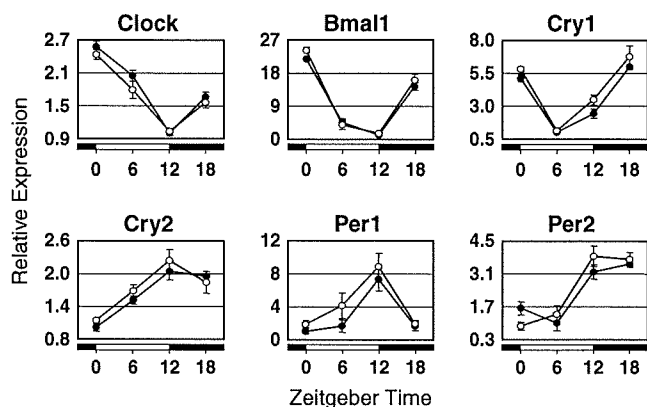

Fig. 1. Daily mRNA expression profiles of clock genes in the livers of mice fed a regular (black circles) or an atherogenic (white circles) diet. Transcript levels of the clock genes were determined by real-time quantitative PCR. Data are means ± SEM of four mice at each time point and are expressed as relative values to the lowest values in control mice for each gene.

As expected, the atherogenic diet altered the mRNA expression of various genes related to energy production, redox regulation, the MAPK cascade, and carbohydrate and lipid metabolism. Additionally, these effects on mRNA expression exhibited daily variation; they became marked during the dark/active phase. Because the light condition and daily feeding profile did not differ between mice fed the atherogenic diet and control mice, the daily variation in the intake of the atherogenic diet components may have caused the difference between mRNA expression profiles in the dark and light phases. However, the intracellular clock remained intact under these drastically altered conditions. These results suggest that the circadian clock is protected against, or not susceptible to, alterations in the intracellular environment, including redox state and metabolism.

Light and dietary intake strongly entrain the master and hepatic clocks, respectively [2,31]. The master clock in the SCN may synchronize the peripheral oscillators, at least partly via the autonomic nervous system [2]. In this study, the mice with NASH were maintained on a well-regulated 12-h light/12-h dark cycle. Additionally, their daily feeding rhythm did not differ from that of control mice (data not shown). Under this condition, the hepatic clock ticked normally. Kohsaka et al. [13] reported that a high-fat diet lengthened the period of locomotor activity rhythm under constant darkness in mice, but the effect was not detected under a 12-h light/12-h dark cycle. Moreover, night-time restricted feeding can normalize the impaired circadian clock in the livers of db/db mice [34]. These results suggest that the signals induced by light and feeding can entrain the hepatic circadian clock, even in the face of the alterations of metabolism and redox state. The influence of a high-fat diet on the hepatic clock may have been observed by Kohsaka et al. [13], but not us [16], due to differences in daily feeding rhythm, which was dampened in their study but not in ours.

Consistent with the intact intracellular clock, the daily expression rhythms of most circadianly expressed genes examined were preserved in the livers of mice with NASH. However, the 24-h expression rhythms of some genes were blunted or changed by the atherogenic diet. It is interesting that the expression rhythms of genes involved in protein degradation were markedly changed in the mice with NASH. The clock proteins, as well as the other short-lived proteins, are degraded by the ubiquitin-proteasome system [2]. Degradation rates of the clock proteins are controlled by their phosphorylation [2] and binding to an F-box protein [35]. These post-translational regulation mechanisms may account for the fact that Cry2 protein accumulates with a markedly higher circadian amplitude than *Cry2* mRNA [36]. Further studies are needed to determine whether the degradation rates of clock proteins are altered to compensate for the effects of the atherogenic diet.

In conclusion, the atherogenic diet caused NASH and alterations in the intracellular environment, affecting energy metabolism, protein degradation, and redox state. However, these conditions did not impair the circadian clock or the expression rhythms of most of the genes examined in the liver. These findings provide evidence that the circadian clock is protected against alterations in the intracellular environment, including metabolism and redox state. The impairment of biological clock appears to be important as a cause of metabolic disease.
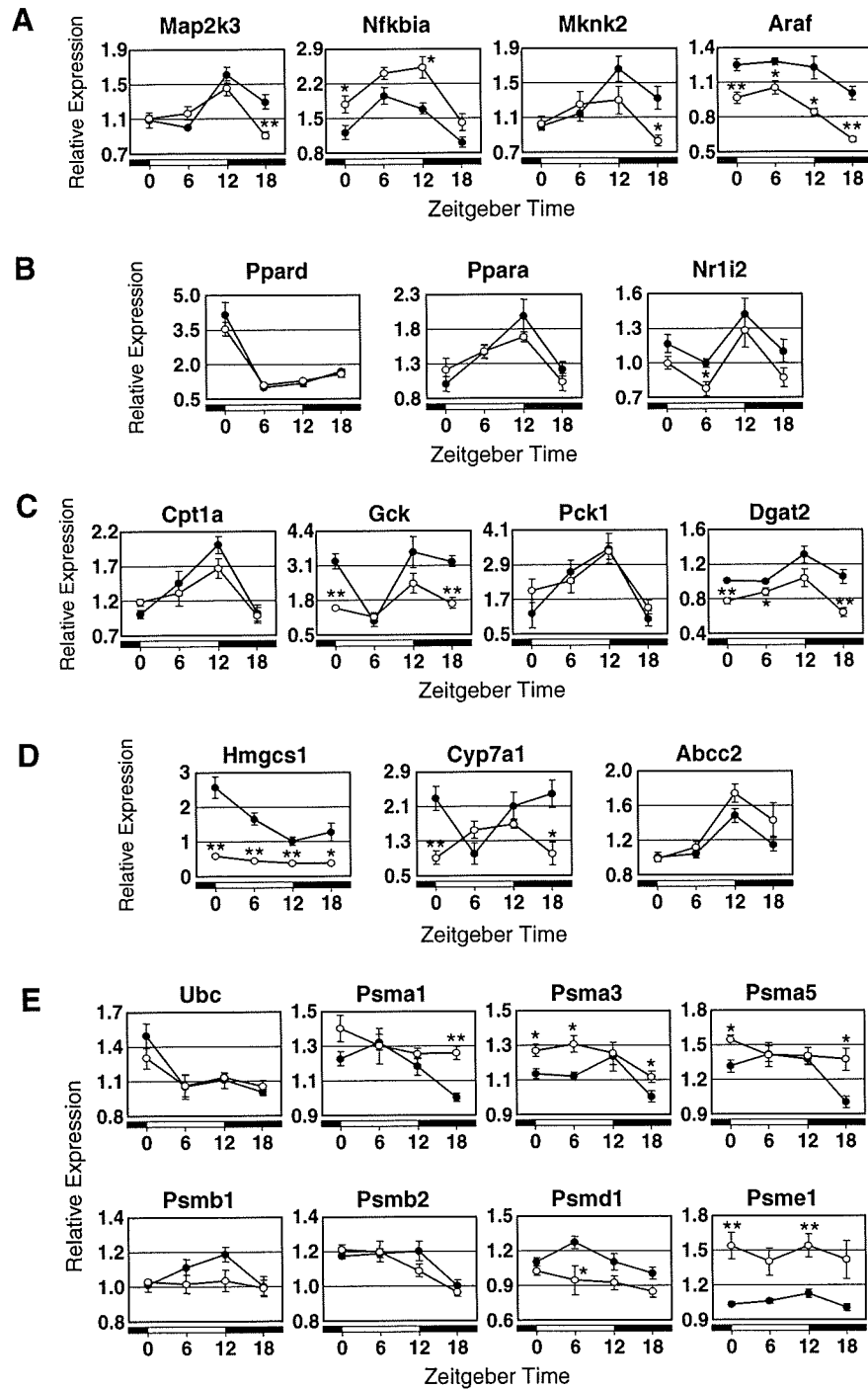
Fig. 2. Daily mRNA expression profiles of the circadianly expressed genes related to the MAPK cascade (A), nuclear receptors (B), energy metabolism (C), cholesterol metabolism (D), and protein degradation (E) in the livers of mice fed a regular (black circles) or an atherogenic (white circles) diet. Transcript levels of the clock genes were determined by the custom-made, high-precision DNA chip. Data are means ± SEM of four mice at each time point and are expressed as relative values to the lowest value in control mice for each gene. $^*P < 0.05$, $^{**}P < 0.01$, vs. control mice.

Appendix A. Supplementary data

Supplementary data associated with this article can be found, in the online version, at doi:10.1016/j.bbrc.2009.01.150.

References

[1] P.L. Lowrey, J.S. Takahashi, Mammalian circadian biology: elucidating genome-wide levels of temporal organization, Annu. Rev. Genomics Hum. Genet. 5 (2004) 407–441.

[2] S.M. Reppert, D.R. Weaver, Coordination of circadian timing in mammals, Nature 418 (2002) 935–941.

[3] S.H. Yoo, S. Yamazaki, P.L. Lowrey, K. Shimomura, C.H. Ko, E.D. Buhr, S.M. Siepka, H.K. Hong, W.J. Oh, O.J. Yoo, M. Menaker, J.S. Takahashi, PERIOD2::LUCIFERASE real-time reporting of circadian dynamics reveals persistent circadian oscillations in mouse peripheral tissues, Proc. Natl. Acad. Sci. USA 101 (2004) 5339–5346.

[4] X. Yang, M. Downes, R.T. Yu, A.L. Bookout, W. He, M. Straume, D.J. Mangelsdorf, R.M. Evans, Nuclear receptor expression links the circadian clock to metabolism, Cell 126 (2006) 801–810.

[5] F.W. Turek, C. Joshu, A. Kohsaka, E. Lin, G. Ivanova, E. McDearmon, A. Laposky, S. Losee-Olson, A. Easton, D.R. Jensen, R.H. Eckel, J.S. Takahashi, J. Bass, Obesity

and metabolic syndrome in circadian Clock mutant mice, Science 308 (2005) 1043–1045.

[6] H. Ando, H. Yanagihara, Y. Hayashi, Y. Obi, S. Tsuruoka, T. Takamura, S. Kaneko, A. Fujimura, Rhythmic messenger ribonucleic acid expression of clock genes and adipocytokines in mouse visceral adipose tissue, Endocrinology 146 (2005) 5631–5636.

[7] H. Ando, T. Takamura, N. Matsuzawa-Nagata, K.R. Shima, T. Eto, H. Misu, M. Shiramoto, T. Tsuru, S. Irie, A. Fujimura, S. Kaneko, Clock gene expression in peripheral leucocytes of patients with type 2 diabetes, Diabetologia 52 (2009) 329–335.

[8] P.Y. Woon, P.J. Kaisaki, J. Braganca, M.T. Bihoreau, J.C. Levy, M. Farrall, D. Gauguier, Aryl hydrocarbon receptor nuclear translocator-like (BMAL1) is associated with susceptibility to hypertension and type 2 diabetes, Proc. Natl. Acad. Sci. USA 104 (2007) 14412–14417.

[9] E.M. Scott, A.M. Carter, P.J. Grant, Association between polymorphisms in the Clock geneobesity and the metabolic syndrome in man, Int. J. Obes. (Lond.) 32 (2008) 658–662.

[10] S. Sookoian, G. Castano, C. Gemma, T.F. Gianotti, C.J. Pirola, Common genetic variations in CLOCK transcription factor are associated with nonalcoholic fatty liver disease, World J. Gastroenterol. 13 (2007) 4242–4248.

[11] T. Hirota, T. Okano, K. Kokame, H. Shirotani-Ikejima, T. Miyata, Y. Fukada, Glucose down-regulates Per1 and Per2 mRNA levels and induces circadian gene expression in cultured Rat-1 fibroblasts, J. Biol. Chem. 277 (2002) 44244–44251.

[12] J. Rutter, M. Reick, L.C. Wu, S.L. McKnight, Regulation of clock and NPAS2 DNA binding by the redox state of NAD cofactors, Science 293 (2001) 510–514.

[13] A. Kohsaka, A.D. Laposky, K.M. Ramsey, C. Estrada, C. Joshu, Y. Kobayashi, F.W. Turek, J. Bass, High-fat diet disrupts behavioral and molecular circadian rhythms in mice, Cell Metab. 6 (2007) 414–421.

[14] K. Oishi, M. Kasamatsu, N. Ishida, Gene- and tissue-specific alterations of circadian clock gene expression in streptozotocin-induced diabetic mice under restricted feeding, Biochem. Biophys. Res. Commun. 317 (2004) 330–334.

[15] H. Ando, K. Ushijima, H. Yanagihara, Y. Hayashi, T. Takamura, S. Kaneko, A. Fujimura, Clock gene expression in the liver and adipose tissues of non-obese type 2 diabetic Goto-Kakizaki rats, Clin. Exp. Hypertens., in press.

[16] H. Yanagihara, H. Ando, Y. Hayashi, Y. Obi, A. Fujimura, High-fat feeding exerts minimal effects on rhythmic mRNA expression of clock genes in mouse peripheral tissues, Chronobiol. Int. 23 (2006) 905–914.

[17] G.C. Farrell, C.Z. Larter, Nonalcoholic fatty liver disease: from steatosis to cirrhosis, Hepatology 43 (2006) S99–S112.

[18] N. Matsuzawa, T. Takamura, S. Kurita, H. Misu, T. Ota, H. Ando, M. Yokoyama, M. Honda, Y. Zen, Y. Nakanuma, K. Miyamoto, S. Kaneko, Lipid-induced oxidative stress causes steatohepatitis in mice fed an atherogenic diet, Hepatology 46 (2007) 1392–1403.

[19] T. Takamura, M. Sakurai, T. Ota, H. Ando, M. Honda, S. Kaneko, Genes for systemic vascular complications are differentially expressed in the livers of type 2 diabetic patients, Diabetologia 47 (2004) 638–647.

[20] Y. Takeshita, T. Takamura, E. Hamaguchi, A. Shimizu, T. Ota, M. Sakurai, S. Kaneko, Tumor necrosis factor-alpha-induced production of plasminogen activator inhibitor 1 and its regulation by pioglitazone and cerivastatin in a nonmalignant human hepatocyte cell line, Metabolism 55 (2006) 1464–1472.

[21] H. Misu, T. Takamura, N. Matsuzawa, A. Shimizu, T. Ota, M. Sakurai, H. Ando, K. Arai, T. Yamashita, M. Honda, T. Yamashita, S. Kaneko, Genes involved in

oxidative phosphorylation are coordinately upregulated with fasting hyperglycaemia in livers of patients with type 2 diabetes, Diabetologia 50 (2007) 268–277.

[22] Y. Takeshita, T. Takamura, H. Ando, E. Hamaguchi, A. Takazakura, N. Matsuzawa-Nagata, S. Kaneko, Cross talk of tumor necrosis factor-alpha and the renin-angiotensin system in tumor necrosis factor-alpha-induced plasminogen activator inhibitor-1 production from hepatocytes, Eur. J. Pharmacol. 579 (2008) 426–432.

[23] T. Takamura, H. Misu, N. Matsuzawa-Nagata, M. Sakurai, T. Ota, A. Shimizu, S. Kurita, Y. Takeshita, H. Ando, M. Honda, S. Kaneko, Obesity upregulates genes involved in oxidative phosphorylation in livers of diabetic patients, Obesity, in press (Epub ahead of print).

[24] T. Takamura, H. Misu, T. Yamashita, S. Kaneko, SAGE application in the study of diabetes, Curr. Pharm. Biotechnol. 9 (2008) 392–399.

[25] A. Shimizu, T. Takamura, N. Matsuzawa, S. Nakamura, S. Nabemoto, Y. Takeshita, H. Misu, S. Kurita, M. Sakurai, M. Yokoyama, Y. Zen, M. Sasaki, Y. Nakanuma, S. Kaneko, Regulation of adiponectin receptor expression in human liver and a hepatocyte cell line, Metabolism 56 (2007) 1478–1485.

[26] H. Ando, Y. Oshima, H. Yanagihara, Y. Hayashi, T. Takamura, S. Kaneko, A. Fujimura, Profile of rhythmic gene expression in the livers of obese diabetic KK-A(y) mice, Biochem. Biophys. Res. Commun. 346 (2006) 1297–1302.

[27] N. Matsuzawa-Nagata, T. Takamura, H. Ando, S. Nakamura, S. Kurita, H. Misu, T. Ota, M. Yokoyama, M. Honda, K. Miyamoto, S. Kaneko, Increased oxidative stress precedes the onset of high-fat diet-induced insulin resistance and obesity, Metabolism 57 (2008) 1071–1077.

[28] M. Uno, S. Kurita, H. Misu, H. Ando, T. Ota, N. Matsuzawa-Nagata, Y. Kita, S. Nabemoto, H. Akahori, Y. Zen, Y. Nakanuma, S. Kaneko, T. Takamura, Tranilast, an antifibrogenic agent, ameliorates a dietary rat model of nonalcoholic steatohepatitis, Hepatology 48 (2008) 109–118.

[29] S. Kurita, T. Takamura, T. Ota, N. Matsuzawa-Nagata, Y. Kita, M. Uno, S. Nabemoto, K. Ishikura, H. Misu, H. Ando, Y. Zen, Y. Nakanuma, S. Kaneko, Olmesartan ameliorates a dietary rat model of non-alcoholic steatohepatitis through its pleiotropic effects, Eur. J. Pharmacol. 588 (2008) 316–324.

[30] R. Hardeland, A. Coto-Montes, B. Poeggeler, Circadian rhythms, oxidative stress, and antioxidative defense mechanisms, Chronobiol. Int. 20 (2003) 921–962.

[31] S. Langmesser, U. Albrecht, Life time-circadian clocks, mitochondria and metabolism, Chronobiol. Int. 23 (2006) 151–157.

[32] K. Obrietan, S. Impey, D.R. Storm, Light and circadian rhythmicity regulate MAP kinase activation in the suprachiasmatic nuclei, Nat. Neurosci. 1 (1998) 693–700.

[33] L. Fu, H. Pelicano, J. Liu, P. Huang, C. Lee, The circadian gene Period2 plays an important role in tumor suppression and DNA damage response in vivo, Cell 111 (2002) 41–50.

[34] T. Kudo, M. Akiyama, K. Kuriyama, M. Sudo, T. Moriya, S. Shibata, Night-time restricted feeding normalises clock genes and Pai-1 gene expression in the db/db mouse liver, Diabetologia 47 (2004) 1425–1436.

[35] L. Busino, F. Bassermann, A. Maiolica, C. Lee, P.M. Nolan, S.I. Godinho, G.F. Draetta, M. Pagano, SCFFbxl3 controls the oscillation of the circadian clock by directing the degradation of cryptochrome proteins, Science 316 (2007) 900–904.

[36] D. Gatfield, U. Schibler, Physiology. Proteasomes keep the circadian clock ticking, Science 316 (2007) 1135–1136.

Enhancement of tumor-specific T-cell responses by transcatheter arterial embolization with dendritic cell infusion for hepatocellular carcinoma

Eishiro Mizukoshi[1], Yasunari Nakamoto[1], Kuniaki Arai[1], Tatsuya Yamashita[1], Naofumi Mukaida[2], Kouji Matsushima[3], Osamu Matsui[4] and Shuichi Kaneko[1]

[1] Department of Disease Control and Homeostasis, Graduate School of Medicine, Kanazawa University, Kanazawa, Japan
[2] Division of Molecular Bioregulation, Cancer Research Institute, Kanazawa University, Kanazawa, Japan
[3] Department of Molecular Preventive Medicine, Graduate School of Medicine, Tokyo University, Tokyo, Japan
[4] Department of Radiology, Graduate School of Medicine, Kanazawa University, Kanazawa, Japan

Transcatheter arterial embolization (TAE) destroys a tumor by the induction of necrosis and/or apoptosis and causes inflammation with cytokine production, which may favor immune activation and presentation of tumor-specific antigens. In the current study, we attempted to identify the effect of TAE on tumor-specific T-cell responses and the additional effect of dendritic cell (DC) infusion performed during TAE. The prevalence of tumor antigen-specific T cells was determined by interferon-γ enzyme-linked immunospot analysis using alpha-fetoprotein (AFP) and tumor antigen-derived peptides in 20 and 13 patients with hepatocellular carcinoma (HCC) who received TAE and TAE with DC infusion, respectively. The increased frequency of AFP-specific T cells was observed in 6 of 20 patients after TAE. It was observed more frequently in patients with DC infusion than in those with TAE alone. However, tumor recurrence was not completely prevented in patients albeit displayed enhanced immune responses. The evidence that the enhanced immune responses were transient and attenuated within 3 months was provided in time-course analysis. In conclusion, TAE with DC infusion enhances the tumor-specific immune responses more effectively than TAE alone. Although the effect is not sufficient to prevent HCC recurrence, these results may contribute to the development of novel immunotherapeutic approach for HCC.

Hepatocellular carcinoma (HCC) is one of the most common malignancies and has gained major clinical interest because of its increasing incidence. Although current advances in therapeutic modalities have improved the prognosis of patients with HCC, the survival rate is still unsatisfactory.[1-4] One of the reasons for the poor prognosis is the high rate of recurrence after treatment.[5] Therefore, the development of new antitumor therapies to protect against recurrence is important to improve the prognosis for HCC.

To protect against recurrence, tumor antigen-specific immunotherapy is an attractive strategy. Several recent studies of cancer treatment causing tumor necrosis or apoptosis have shown that they induce the activation of tumor-specific

immune responses.[6-10] The mechanism to activate host immune responses against tumors is still unknown; however, several studies *in vitro* or *in vivo* suggest that cytokine production, attracting leukocyte infiltration, increase of tumor antigen uptake by macrophages or dendritic cells (DCs) and release of heat shock protein caused by inflammation at the tumor site are associated with the phenomenon.[11-17]

Transcatheter arterial embolization (TAE) has been used extensively in the Western world and Asia to treat unresectable HCCs.[18-20] Although several previous randomized controlled trials have failed to show a survival benefit in patients treated with TAE compared to untreated patients,[21,22] recent studies demonstrated a survival benefit for TAE *versus* conservative treatment in carefully selected patients.[23-25]

Histological assessment of resected HCC after TAE shows that the treatment induces necrotic and apoptotic changes in the tumor.[26-29] Moreover, it is reported that the serum levels of macrophage-colony stimulating factor and the lipopolysaccharide-stimulated production of interleukin-1 beta, IL-6 and tumor necrosis factor-alpha in peripheral whole blood were increased after TAE.[30-32] Taken together with the previously described knowledge of immune responses after treatment to induce tumor necrosis or apoptosis, these observations support the hypothesis that the induction of apoptotic or necrotic cell death and inflammatory cytokines by TAE favors immune activation and induction of tumor-specific T-cell

responses. In a previous study, we also made a preliminary report that immune responses specific for tumor antigens were enhanced after HCC treatments.[7,10] In addition, we have recently developed a new immunotherapeutic approach for HCC using DC infusion performed during TAE, showing the potential to enhance tumor-specific immune responses.[7]

In the current study, we first attempted to identify the effect of TAE for tumor-specific T-cell responses in patients with HCC. Next, we examined the additional effects of DC infusion to the tumor site after TAE. Finally, we analyzed the relationship between clinical characteristics of patients and T-cell responses after TAE and evaluated whether the activation of tumor-specific T-cell responses can prevent HCC recurrence.

Material and Methods
Patient population
The study examined 33 patients with HCC, consisting of 25 men and 8 women ranging from 48 to 83 years old with a mean age of 66 ± 9 years. Twenty patients were treated by TAE. Thirteen patients were treated by TAE with DC infusion as a part of clinical study, which was approved by ethical committee of Kanazawa University Graduate School of Medical Science and registered in September 2003. The patients who received TAE with DC infusion were selected according to the criteria we previously reported.[7] All subjects were negative for Abs to human immunodeficiency virus (HIV) and gave written informed consent to participate in this study in accordance with the Helsinki declaration.

Treatment of hepatocellular carcinoma
HCCs were detected by imaging modalities such as dynamic CT scan, MR imaging and abdominal arteriography. The diagnosis of HCC was histologically confirmed by taking US-guided needle biopsy specimens, surgical resection or autopsy in 18 cases. For the remaining 15 patients, the diagnosis was based on typical hypervascular tumor staining on angiography in addition to typical findings, which showed hyperattenuated areas in the early phase and hypoattenuation in the late phase on dynamic CT.[33] The tumor size was categorized as "small" (≤ 2 cm) or "large" (>2 cm), and tumor multiplicity was categorized as "multiple" (≥ 2 nodules) or "solitary" (single nodule). The TNM stage was classified according to the Union Internationale Contre Le Cancer (UICC) classification system (6th version).[34]

Twenty patients were treated by TAE as previously described.[19,35] In brief, after evaluation of the feeding arteries and surrounding vascular anatomy, a microcatheter (Microferret, Cook, Bloomington, IN) was inserted into the segmental or subsegmental artery with a coaxial method using a 0.016-inch guidewire (Radifocus GT wire, Terumo, Tokyo, Japan). A mixture of the anticancer drug and iodized oil was administered, and the feeding artery was embolized with gelatin sponge particles (Gelfoam; Pharmacia Upjohn, Kalaman-

zoo, MI). The mixture of anticancer drug and iodized oil contained 10–30 mg of Epirubicin (Farmorubicin; Kyowa Hakko Kogyo, Tokyo, Japan), 1–3 ml of iodized oil (Lipiodol Ultra Fluide) and 0.5–1.0 ml of iohexol (Omnipaque 300).

Preparation and injection of autologous DCs
DCs were generated as previously described.[7] In 6 patients, DCs were pulsed with 0.1 KE/ml OK-432 (Chugai Pharmaceutical, Tokyo, Japan), which is a biological response modifier derived from the weakly virulent Su strain of Streptococcus pyogenes,[36,37] for 3 days before injection. The cells were harvested for injection; 5×10^6 cells were reconstituted in 5-ml normal saline containing 1% autologous plasma, mixed with gelatin sponge particles and infused through an arterial catheter following iodized oil injection during TAE.

After TAE or TAE with DC infusion, 26 patients received percutaneous tumor ablation by ethanol injection (PEIT), microwave coagulation (MCT) or radiofrequency (RF). Twenty-one patients were diagnosed with complete necrosis of the tumor lesion using dynamic CT after the completion of treatment. Follow-ups were conducted at outpatient clinics using blood tests and dynamic CT every 3 months for 1 year.

Laboratory and virologic testing
Blood samples were tested for HBsAg and HCVAb by commercial immunoassays (Fuji Rebio, Tokyo, Japan). HLA-based typing of PBMC from patients was performed using complement-dependent microcytotoxicity with HLA typing trays purchased from One Lambda. The serum alpha-fetoprotein (AFP) level was measured by enzyme immunoassay (AxSYM AFP, Abbott Japan, Tokyo, Japan), and the pathological grading of tumor cell differentiation was assessed according to the general rules for the clinical and pathologic study of primary liver cancer.[38] The severity of liver disease (stage of fibrosis) was evaluated according to the criteria of Desmet et al.[39]

Interferon-γ enzyme-linked immunospot assay
The prevalence of tumor antigen-specific T cells was determined by interferon (IFN)-γ enzyme-linked immunospot (ELISPOT) analysis (Mabtech, Nacka, Sweden) as previously described.[10,40] HLA-A24-restricted AFP-derived peptides (10 μg/ml), which were AFP$_{357}$ (EYSRRHPQL), AFP$_{403}$ (KYIQESQAL) and AFP$_{434}$ (AYTKKAPQL),[10] and 20 μg/ml AFP derived from human placenta (Morinaga Institute of Biological Science, Yokohama, Japan, purity >98%) were added directly to the wells. These 3 AFP-derived peptides could induce CTLs showing cytotoxicity against hepatoma cells and were frequently recognized by PBMCs of patients with HCC as we previously reported,[10] and therefore, we selected them as an immunogenic peptide. The HLA-A24-restricted AFP and CMV-derived peptides were used only for HLA-A24 or A23 positive patients. Other tumor antigen-derived peptides consisted of MRP3$_{503}$ (LYAWEPSFL), MRP3$_{692}$ (AYVPQQAWI), MRP3$_{765}$ (VYSDADIFL), hTERT$_{167}$ (AYQVCGPPL), hTERT$_{324}$

(VYAETKHFL) and $hTERT_{461}$ (VYGFVRACL), which we previously reported that they were useful for analyzing host immune responses to HCC.[40,41]

PBMCs were added to the wells at 3×10^5 cells/well. In the assay using PBMC depleted $CD4^+$ or $CD8^+$ cells, the number of cells was adjusted to 3×10^5 cells/well after the depletion. Depletion of $CD4^+$ or $CD8^+$ cells was performed by MACS separation system using CD4 or CD8 MicroBeads (Miltenyi Biotec, Auburn, CA) in accordance with the manufacturer's instructions. After the depletion, 1×10^6 cells were stained with CD4 and CD8 antibodies (Becton Dickinson, Tokyo, Japan) and analyzed by FACSCalibur (Becton Dickinson, Tokyo, Japan) to confirm the ratio of $CD4^+$ and $CD8^+$ cells. Data analysis was undertaken with CELLQuest™ software (Becton Dickinson, San Jose, CA).

Plates were analyzed with a KS ELISpot Reader (Zeiss, Tokyo, Japan). The number of specific spots was determined by subtracting the number of spots in the absence of antigen. Responses were considered positive if more than 10 specific spots were detected and if the number of spots in the presence of antigen was at least 2-fold greater than the number of spots in the absence of antigen. Negative controls consisted of incubation of PBMCs with a peptide representing an HLA-A24-restricted epitope derived from HIV envelope protein ($HIVenv_{584}$) and were always <5 spots per 3×10^5 cells.[42] The positive controls consisted of 10 ng/ml phorbol 12-myristate 13-acetate (PMA, Sigma) or a CMV pp65-derived peptide ($CMVpp65_{328}$).[43] All peptides used in this study were synthesized at Sumitomo Pharmaceuticals (Osaka, Japan). ELISPOT analysis was performed before and 2–4 weeks after TAE. In patients receiving additional treatment for complete ablation of tumor, analysis was performed just before the additional treatment. An increase of antigen-specific T cells was defined as significant when T-cell responses changed to positive or if the number of spots detected after TAE was at least 2-fold greater than the number of spots detected before treatment.

Statistical analysis

Unpaired Student's *t*-test was used to analyze the effect of variables on immune responses in patients with HCC. Fisher's exact test (2-sided *p*-value) was used to analyze the frequency of positive immune responses in patients between with TAE and TAE with DC infusion.

Results

T-cell responses to AFP in the patients who received TAE

The frequency of AFP-specific T cells before and after TAE was tested *ex vivo* in an IFN-γ ELISPOT assay. The serum AFP level and number of peripheral lymphocytes and antigen-specific T cells are shown in Table 1. Before treatment, 2 patients showed a specific T-cell response to AFP-derived peptides and 3 patients to protein in 20 patients (Patients 1–20). After treatment, a T-cell response to AFP-derived pep-

tides and protein was detected in 4 and 3 patients, respectively.

When an increase of antigen-specific T cells was defined as significant if T-cell responses changed to positive or the number of spots detected after TAE was at least 2-fold greater than the number of spots detected before treatment, 6 of 20 (30%) patients (Patients 4, 6, 7, 11, 18 and 20) showed a significant increasing of AFP-specific T-cell frequency after treatment. It was observed even in the patient (Patients 6, 7 and 18) who had no T cells specific to corresponding AFP-derived peptides before treatment. When a decrease of antigen-specific T cells was defined as significant if T-cell responses changed from positive to negative or the number of spots detected after TAE was less than half of the number of spots detected before treatment, 4 of 20 (20%) patients (Patients 5, 14, 15 and 16) showed a significant decreasing of AFP-specific T-cell frequency after treatment.

AFP-specific IFN-γ-producing T cells were also analyzed by ELISPOT assay using PBMC depleted $CD4^+$ or $CD8^+$ cells to determine what kind of T cells is responsive to whole AFP. Depletion of $CD4^+$ or $CD8^+$ cells was performed by MACS separation system, and the results were confirmed by flow cytometric analysis (Fig. 1*a*). After depletion of $CD4^+$ or $CD8^+$ cells, the ratio of each cell population was decreased to less than 0.1% of PBMCs. The IFN-γ ELISPOT assay showed that IFN-γ-producing T cells against AFP consisted of both $CD8^+$ and $CD4^+$ cells (Fig. 1*b*).

To confirm the effect of TAE for host immune responses to HCC, we also examined the frequency of tumor antigen-specific T cells in 4 patients (Patients 5, 8, 10 and 14) using MRP3- or hTERT-derived peptides that we previously identified as useful for analyzing host immune responses to HCC.[40,41] A significant increasing of MRP3- or hTERT-specific T-cell frequency was observed in all patients after TAE (Table 2).

T-cell responses to AFP in the patients who received TAE with DC infusion

In 13 patients receiving TAE with DC infusion (Patients 21–33), 2 patients showed a specific T-cell response with AFP-derived peptides and 2 patients with protein before treatment (Table 3). After treatment, 8 patients showed a specific T-cell response to AFP-derived peptides and 3 patients to protein.

Next, we compared TAE with DC infusion with TAE alone regarding the effect to AFP-specific immune response. Table 4 shows the clinical features of patients with HCC who received TAE and TAE with DC infusion and they were not statistically different except liver function.

The frequency of patients who showed both positive and increasing T-cell response with AFP-derived peptides or protein after treatment was significantly higher in patients receiving TAE with DC infusion than in those receiving TAE alone (*p* = 0.04) (Fig. 2*a*). On the other hand, the frequency of patients who showed both positive and increasing T-cell

Table 1. T cell response to AFP and AFP-derived peptides by ELISPOT assay before and after TAE

Patient	HLA	Additional treatment	Complete ablation	Before treatment								After treatment							
				AFP (ng/ml)	Lymph. (µl⁻¹)	AFP$_{357}$	AFP$_{403}$	AFP$_{434}$	AFP	CMVpp65$_{328}$	TT	AFP (ng/ml)	Lymph. (µl⁻¹)	AFP$_{357}$	AFP$_{403}$	AFP$_{434}$	AFP	CMVpp65$_{328}$	TT
1	A2	RF	C	<10	1,600	ND	ND	ND	1	ND	0	<10	1,400	ND	ND	ND	0	ND	1
2	A26,A31	RF	C	61	1,700	ND	ND	ND	0	ND	13	23	900	ND	ND	ND	0	ND	0
3	A11,A26	No	–	100	1,700	ND	ND	ND	5	ND	1	50	1,500	ND	ND	ND	0	ND	0
4	A24	RF	C	18	700	0	7	0	6	0	25	16	500	1	10	1	1	2	16
5	A24,A33	RF	C	2,357	1,200	13	2	6	0	13	0	700	1,100	2	1	1	0	9	0
6	A24	RF	C	14	1,800	0	0	0	0	0	42	<10	1,400	53	27	38	14	36	108
7	A23,A33	No	–	96	500	0	0	0	5	291	0	138	800	46	0	0	3	484	0
8	A24,A26	No	–	142	600	1	0	0	0	0	0	126	500	2	0	0	0	166	1
9	A2,A24	RF	C	<10	700	6	1	0	0	9	0	<10	700	0	0	0	0	32	15
10	A24	PEIT	C	<10	1,300	8	4	8	8	146	5	<10	1,300	0	1	1	0	1	1
11	A24,A26	PEIT	N	18	1,100	0	0	0	1	ND	0	13	400	0	0	0	15	10	55
12	A24,A33	RF	N	11	800	3	2	0	4	94	10	11	700	0	0	0	0	24	0
13	A11,A24	PEIT	C	52	1,300	0	2	5	1	2	0	24	1,200	0	0	0	0	0	3
14	A24	RF	C	54	2,400	25	5	4	8	12	0	67	1,700	0	0	0	0	0	0
15	A2,A24	RF	N	62	1,200	0	3	0	25	2	3	14	800	0	0	0	8	0	0
16	A3,A24	RF	C	2,876	900	0	1	0	13	0	5	3,285	700	0	0	0	0	0	0
17	A24,A33	No	–	205	400	4	2	3	2	26	9	220	100	2	1	0	1	39	1
18	A24,A30	RF	C	18	1,100	4	0	3	8	14	7	13	900	1	16	1	5	12	0
19	A2,A24	RF	C	330	1,500	2	0	0	0	18	1	36	1,100	0	4	0	3	8	1
20	A2,A33	RF	C	10	1,400	ND	ND	ND	10	ND	68	<10	800	ND	ND	ND	31	ND	101

Abbreviations: Lymph., number of lymphocytes; RF, radiofrequency ablation; PEIT, percutaneous ethanol injection therapy; No, no treatment; C, completed; N, not completed; –, not done. The bold letters show the positive responses in ELISPOT assays.
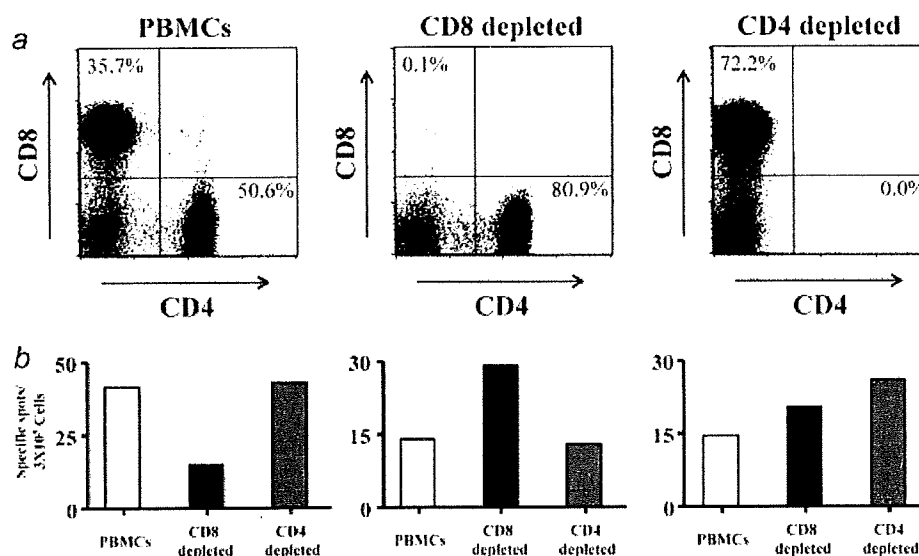
Figure 1. IFN-γ production of CD4- or CD8-depleted T cells against whole AFP. AFP-specific IFN-γ-producing T cells were analyzed by ELISPOT assay using PBMC depleted CD4$^+$ or CD8$^+$ cells to determine what kind of T cells is responsive to whole AFP. Depletion of CD4$^-$ or CD8$^+$ cells was performed by MACS separation system and the results were confirmed by flow cytometric analysis (*a*). IFN-γ ELISPOT assay using nontreated PBMCs and PBMC depleted CD4$^+$ or CD8$^-$ cells showed that T cells producing IFN-γ against whole AFP consisted of both CD8$^+$ and CD4$^+$ cells (*b*). Assays were performed in 5 patients and the representative result is shown.

Table 2. T cell response to other tumor antigen-derived peptides by ELISPOT assay before and after TAE

Patient	Before treatment						After treatment					
	MRP3$_{503}$	MRP3$_{692}$	MRP3$_{765}$	hTERT$_{167}$	hTERT$_{324}$	hTERT$_{461}$	MRP3$_{503}$	MRP3$_{692}$	MRP3$_{765}$	hTERT$_{167}$	hTERT$_{324}$	hTERT$_{461}$
5	2	7	8	0	3.5	7.5	0	0	0	**7**	3	**35**
8	6	6	1	3	ND	ND	**17**	**18**	**22**	**18**	**14**	**9**
10	0	1	3	0	5	7	0	4	**7**	**6**	**11**	4
14	6	5	0	**9**	5	**13**	6	**14**	**22**	**8**	**10**	7

Abbreviation: ND, not done. The bold letters show the positive responses in ELISPOT assays.

response with CMV-derived peptide or tetanus toxoid was not different between the 2 groups (Figs. 2*b* and 2*c*).

In the comparison of the mean values of spots generated with AFP-derived peptides, protein, CMV-derived peptides or tetanus toxoid, no significant difference was observed between patients with TAE alone before and after treatment (Figs. 3*a*–3*d*). In contrast, the mean values of spots generated with AFP-derived peptides were significantly higher in patients after TAE with DC infusion than in those before treatment (Fig. 3*e*). The mean values of spots generated with protein, CMV-derived peptides or tetanus toxoid were not significantly different between patients before and after TAE with DC infusion (Figs. 3*f*–3*h*). Based on the above results, we considered that the main difference between TAE alone and TAE with DC infusion was the response to HLA-A24-restricted AFP-derived epitopes. Therefore, to analyze the difference between TAE alone and TAE with DC infusion more precisely, we selected the patients with HLA-A24 or A23 and

compared the clinical parameters of both groups. However, there were no statistical differences except liver function in the 2 groups (Table 5).

Enhancement of AFP-specific T-cell responses and treatment outcome

To evaluate the effect of immune enhancement by TAE or TAE with DC infusion for the treatment outcome, we analyzed the clinical course of 17 patients who received complete ablation by additional RFA, PEIT or MCT after these treatments and could be followed up using dynamic CT every 3 months (Table 6). Seven patients showed increasing specific spots for AFP or AFP-derived peptides in ELISPOT assay after TAE. HCC recurrence within 3 months after complete ablation was observed in 3 patients who showed increasing AFP-specific T-cell responses after TAE. Furthermore, recurrence within 6 months after complete ablation was observed

Tumor Immunology

Table 3. T cell response to AFP and AFP-derived peptides by ELISPOT assay before and after TAE with DC infusion

Patient	HLA	Additional treatment	Complete ablation	Before treatment								After treatment							
				AFP (ng/ml)	Lymph. (µl⁻¹)	AFP$_{357}$	AFP$_{403}$	AFP$_{434}$	AFP	CMVpp65$_{328}$	TT	AFP (ng/ml)	Lymph. (µl⁻¹)	AFP$_{357}$	AFP$_{403}$	AFP$_{434}$	AFP	CMVpp65$_{328}$	TT
21	A24	No	–	332	1,100	7	1	4	ND	10	ND	819	800	11	0	10	ND	188	ND
22	A24,A26	RF	N	341	700	0	**26**	5	ND	**68**	ND	237	500	ND	**59**	ND	ND	**81**	ND
23	A11,A24	No	–	41	600	0	2	5	1	2	0	43	400	0	0	0	0	0	3
24	A2,A24	MCT	C	1,260	800	3	8	7	ND	**19**	ND	614	1,300	**26**	4	7	ND	**12**	**4**
25	A24,A33	RF	C	11	1,500	0	1	0	**31**	5	**15**	19	900	1	4	**15**	**26**	3	**4**
26	A24,A33	RF	C	<10	2,000	0	0	0	0	0	0	<10	1,700	0	**16**	0	0	0	1
27	A24,A26	RF	C	16	700	0	0	0	1	1	0	16	700	2	1	**15**	**9**	0	0
28	A11,A31	RF	N	31	800	ND	ND	ND	3	ND	0	33	700	ND	ND	ND	0	ND	0
29	A11,A33	No	–	<10	1,100	ND	ND	ND	0	ND	0	<10	700	ND	ND	ND	0	ND	1
30	A2,A11	RF	C	13	1,300	ND	ND	ND	8	ND	1	14	1,500	ND	ND	ND	**12**	ND	7
31	A24,A33	RF	C	1,014	800	0	0	0	0	1	0	15	300	0	0	**20**	0	0	0
32	A11,A24	RF	C	<10	1,000	3	3	**11**	**48**	**97**	0	10	1,200	**23**	**20**	**20**	**45**	**91**	**23**
33	A2,A26	RF	C	29	1,300	ND	ND	ND	0	ND	0	27	1,300	ND	ND	ND	0	ND	0

Abbreviations: Lymph., number of lymphocytes; RF, radiofrequency ablation; PEIT, percutaneous ethanol injection therapy; MCT, microwave coagulation therapy; C, completed; N, not completed; –, not determined; ND, not done. The bold letters show the positive responses in ELISPOT assays.

Table 4. Patient characteristics

	Patients treated by TAE (*n* = 20)	Patients treated by TAE with DC (*n* = 13)	*p*-value[1]
Age (years)[2]	66.6 ± 7.8	65.7 ± 10.0	NS
Sex (M/F)	14/6	11/2	NS
HLA (A23 or 24/others)	16/4	9/4	NS
ALT (IU/l)	51.0 ± 47.4	86.9 ± 62.8	NS
Total bilirubin (g/dl)	1.3 ± 0.9	1.5 ± 0.9	NS
Albumin (g/dl)	3.7 ± 0.7	3.2 ± 0.6	NS
AFP level (ng/ml)	322.7 ± 793.0	239.8 ± 418.2	NS
Diff. degrees of HCC (well/moderate or poor/ND[1])	2/6/12	4/4/5	NS
Tumor size (small/large[3])	4/16	1/12	NS
Tumor multiplicity (multiple/solitary)	18/2	12/1	NS
TNM stage (I, II/III, IV)	19/1	11/2	NS
Histology of nontumor liver (LC/chronic hepatitis)	15/5	10/3	NS
Liver function (Child A/B or C)	14/6	3/10	0.02
Etiology (HCV/HBV/others)	12/2/6	13/0/0	NS

[1]Abbreviations: NS, no statistical significance; ND, not determined. [2]Data are expressed as the mean ± SD. [3]Small: ≤2 cm, large: >2 cm.
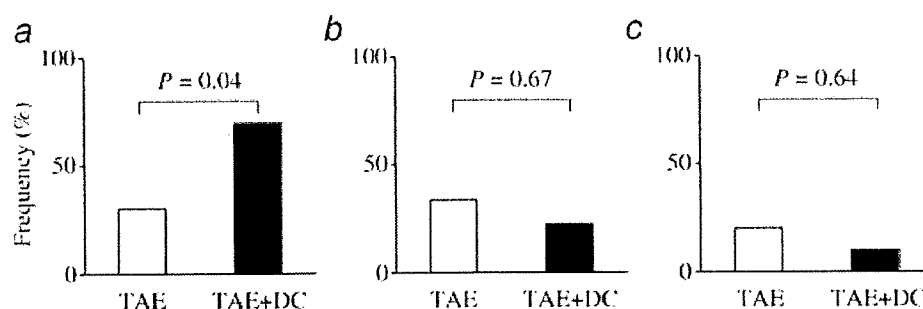
Figure 2. Frequency of the patients who showed enhancement of T-cell responses after treatment. The prevalence of antigen-specific T cells was determined by IFN-γ ELISPOT analysis using alpha-fetoprotein (AFP) and AFP-derived peptides (*a*), CMV pp65-derived peptide (*b*) or tetanus toxoid protein (*c*) in 20 and 13 patients with HCC who received TAE and TAE with DC infusion, respectively.

in 4 and 6 patients who did and did not show increasing AFP-specific T-cell responses, respectively.

Kinetics of AFP-specific T-cell responses before and after TAE

Next, we examined the kinetics of AFP-specific T cells in 8 patients who showed increasing frequency of IFN-γ-producing T cells against AFP or AFP-derived peptides after TAE. The frequency was examined by ELISPOT assay before and 2–4 weeks and 3 months after TAE. Thirteen kinds of AFP-specific T cells showed increasing frequency 2–4 weeks after TAE (Fig. 4); however, the increase was transient and most cell types decreased 3 months after TAE. Three patients showed more than 10 specific spots for AFP or AFP-derived peptides 3 months after TAE (Patients 6, 11 and 30). In analysis of the correlation between the maintenance of AFP-specific T-cell responses and HCC recurrence, 1 patient (Patient

6) had HCC recurrence after 6 months and 1 patient (Patient 30) did not show recurrence. Another patient (Patient 11) did not receive curative ablation and was not analyzed. There was no difference in the kinetics of AFP-specific T cells between patients who received TAE with and without DC infusion.

Discussion

In a previous study, we made a preliminary report that immune responses specific for tumor antigens were enhanced after HCC treatments.[7,10] Similarly, as in our previous or other group's results,[8] we observed enhancement of AFP-specific immune responses in 6 of 20 patients with TAE alone in this study. The enhancement of tumor antigen-specific immune responses was also observed in the cases using MRP3- or hTERT-derived peptides.
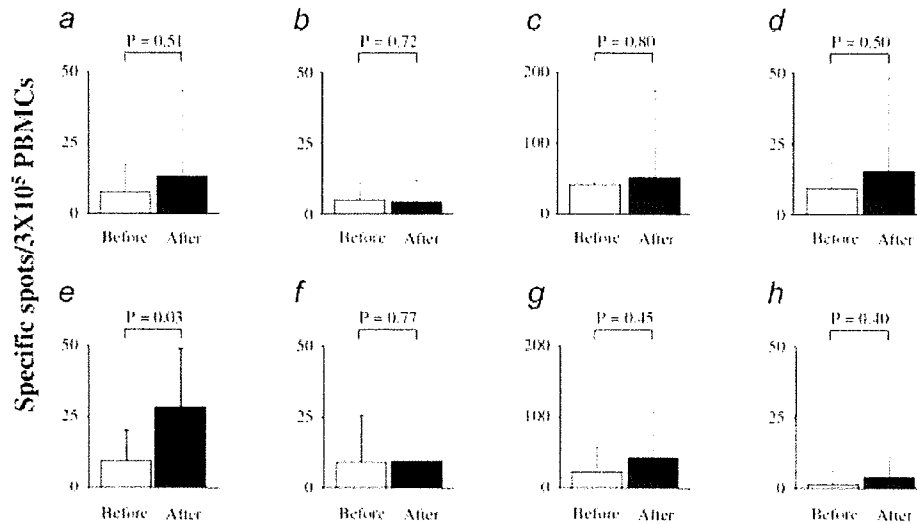
Figure 3. Comparison of direct *ex vivo* analysis (IFN-γ ELISPOT assay) before and after treatment of HCC. The assay was performed using PBMCs of patients who received TAE for AFP-derived peptides (*a*), AFP (*b*), CMV pp65-derived peptide (*c*) or tetanus toxoid protein (*d*). The same assay was performed using PBMCs of patients who received TAE with DC infusion for AFP-derived peptides (*e*), AFP (*f*), CMV pp65-derived peptide (*g*) or tetanus toxoid protein (*h*). AFP and CMV pp65-derived peptides were tested in only HLA-A24 or A23 positive patients. Data are expressed as the mean + SD of specific spots.

Table 5. Characteristics of the patients with HLA-A24 or A23

	Patients treated by TAE (*n* = 16)	Patients treated by TAE with DC (*n* = 9)	*p*-value[1]
Age (years)[2]	65.7 ± 7.8	67.8 ± 10.8	NS
Sex (M/F)	10/6	7/2	NS
ALT (IU/l)	55.9 ± 51.9	75.4 ± 53.0	NS
Total bilirubin (g/dl)	1.4 ± 0.8	1.4 ± 1.1	NS
Albumin (g/dl)	3.6 ± 0.7	3.1 ± 0.6	NS
AFP level (ng/ml)	392.1 ± 877.8	337.2 ± 477.1	NS
Diff. degree of HCC (well/moderate or poor/ND[1])	2/5/9	3/3/3	NS
Tumor size (small/large[3])	3/13	0/9	NS
Tumor multiplicity (multiple/solitary)	15/1	8/1	NS
TNM stage (I, II/III, IV)	15/1	7/2	NS
Histology of nontumor liver (LC/chronic hepatitis)	13/3	8/1	NS
Liver function (Child A/B or C)	10/6	0/9	0.003
Etiology (HCV/HBV/others)	11/1/4	9/0/0	NS

[1]Abbreviations: NS, no statistical significance; ND, not determined. [2]Data are expressed as the mean ± SD. [3]Small: ≤2 cm, large: >2 cm.

The precise mechanism of this phenomenon is still unknown; however, in recent studies, several treatments to destroy tumor cells by necrosis and/or apoptosis have induced antitumor immune responses in animal models[14,44] and even in humans.[6–10] In the study of *in situ* tumor ablation, it is reported that tumor ablation creates a tumor antigen source for the induction of antitumor immunity.[9,44] In another study regarding photodynamic therapy (PDT),[45] it is reported that acute inflammation, expression of heat-shock proteins and providing tumor antigens to DCs caused by PDT induce tumor-specific immune responses.

Based on these results, we hypothesize that DC infusion with TAE can induce antitumor immune responses more effectively than TAE alone. According to DC research in recent years, successful enhancement of the antitumor immune response has been reported by intratumoral

Table 6. Enhancement of AFP-specific T cell response and treatment outcome

	Enhancement of AFP-specific T cell response	Recurrence, 3 months	Recurrence, 6 months
Patient 1	−	N	U
Patient 2	−	N	M
Patient 4	+	M	ND
Patient 5	−	N	M
Patient 6	+	N	U
Patient 9	−	N	M
Patient 10	−	N	N
Patient 13	−	N	N
Patient 14	−	N	N
Patient 16	−	N	M
Patient 19	−	N	U
Patient 24	+	U	ND
Patient 25	+	M	ND
Patient 26	+	N	N
Patient 30	+	N	N
Patient 31	+	N	N
Patient 33	−	N	N

Abbreviations: N, no recurrence; U, uninodular recurrence; M, multinodular recurrence; ND, not determined.

Figure 4. Kinetics of AFP-specific T-cell responses determined by IFN-γ ELISPOT assay before and after TAE. PBMCs were obtained before and 2–4 weeks and 3 months after TAE. Each graph indicates the kinetics of T cells specific for each antigen in each patient. Some patients received additional treatments as indicated in Tables 1 and 3 for a curative treatment after the measurement of T-cell responses at 2–4 weeks after TAE.

administration of DC in combination with tumor ablation.[46,47] Furthermore, immunotherapies using DC have been performed in patients with HCC and their antitumor effects are reported.[48–50] These results support our hypothesis and therefore, in the next step, we examined the immunological effects of DC infusion with TAE.

The comparison of frequency in patients who showed enhancement of AFP-specific immune responses revealed more frequency in patients with DC infusion than in those with TAE alone. On the other hand, there were no differences in the 2 groups in the comparison of frequency for patients who showed enhancement of CMV or TT-specific immune responses. These results suggest that DC infusion with TAE affects tumor-specific immune responses and that the effects are limited to the tumor area.

Some patients with TAE alone showed disappearance of AFP- or control antigen-specific T cells. Although the mechanism of this phenomenon is unknown, anticancer drugs used in TAE might suppress the immune responses, because most of the patients showed decreasing the number of lymphocytes after TAE. These results suggest that TAE alone might give a chance to enhance tumor-specific T-cell responses in only some patients. Further analysis using many more patients with TAE is necessary to make clear the differences in the patients with and without enhancement of T-cell responses. In contrast, disappearance of AFP- or control antigen-specific
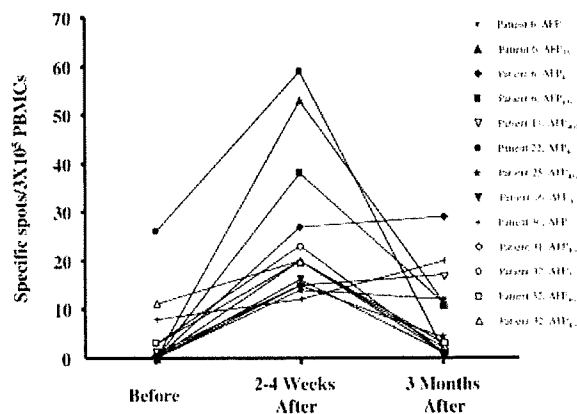
T cells was not observed in the patients with DC infusion, suggesting strong immunostimulating effect of this treatment.

In analysis of the association between the enhancement of AFP-specific T cells and clinical responses, no correlation could be shown, suggesting that enhancement of T-cell response associated with TAE or TAE with DC infusion may not have protective effect against HCC recurrence. To clarify the mechanism in more detail, we examined the kinetics of AFP-specific T-cell response. Increased frequency of AFP-specific T cells was transient and fell in 4 of 8 patients 3 months after treatment (Fig. 4). Similar to our results, Ayaru *et al.* also reported that the frequency of AFP-specific CD4^{+} T cells fell in all patients by 1–3 months after TAE.[8] In addition, our results suggest that DC infusion with TAE is not effective to maintain the increased frequency of AFP-specific T cells.

Recent genome profiling studies of HCC show that HCC is a very heterogenous tumor.[51] Furthermore, HCC has multicentric carcinogenesis and develops at different time points. These characters of HCC may also be another reason for no correlation between the enhancement of AFP-specific T cells and clinical responses. The identification of many more tumor antigens and their T-cell epitopes is necessary for more precise analysis of the relationship between antitumor immune response and clinical response, and for immunotherapy.

In the recent study, it is reported that CD8^{+} T-cell response to AFP is multispecific and AFP-specific IFN-γ-producing CD8^{+} T cells are directed against different epitopes spreading over the entire AFP sequence with no single

immuno-dominant CD8[1] T-cell epitope.[52] Therefore, there is a limitation to our study, because the number of immunogenic AFP-derived peptides applicable in this study is small. However, the results of the present study suggest that TAE with DC infusion enhances the tumor-specific immune responses. Although these modified immune responses may not be sufficient to prevent HCC recurrence because the enhanced immune responses are transient and attenuate within 3 months, these results may contribute to the development of novel immunotherapeutic approach for HCC.

Acknowledgements

References

1. Curley SA, Izzo F, Ellis LM, Nicolas Vauthey J, Vallone P. Radiofrequency ablation of hepatocellular cancer in 110 patients with cirrhosis. *Ann Surg* 2000;232: 381–91.
2. Mazzaferro V, Regalia E, Doci R, Andreola S, Pulvirenti A, Bozzetti F, Montalto F, Ammatuna M, Morabito A, Gennari L. Liver transplantation for the treatment of small hepatocellular carcinomas in patients with cirrhosis. *N Engl J Med* 1996;334: 693–9.
3. Urabe T, Kaneko S, Matsushita E, Unoura M, Kobayashi K. Clinical pilot study of intrahepatic arterial chemotherapy with methotrexate, 5-fluorouracil, cisplatin and subcutaneous interferon-alpha-2b for patients with locally advanced hepatocellular carcinoma. *Oncology* 1998; 55:39–47.
4. Ishizaki Y, Kawasaki S. The evolution of liver transplantation for hepatocellular carcinoma (past, present, and future). *J Gastroenterol* 2008;43:18–26.
5. Okuwaki Y, Nakazawa T, Shibuya A, Ono K, Hidaka H, Watanabe M, Kokubu S, Saigenji K. Intrahepatic distant recurrence after radiofrequency ablation for a single small hepatocellular carcinoma: risk factors and patterns. *J Gastroenterol* 2008;43:71–8.
6. Abdel-Hady ES, Martin-Hirsch P, Duggan-Keen M, Stern PL, Moore JV, Corbitt G, Kitchener HC, Hampson IN. Immunological and viral factors associated with the response of vulval intraepithelial neoplasia to photodynamic therapy. *Cancer Res* 2001;61:192–6.
7. Nakamoto Y, Mizukoshi E, Tsuji H, Sakai Y, Kitahara M, Arai K, Yamashita T, Yokoyama K, Mukaida N, Matsushima K, Matsui O, Kaneko S. Combined therapy of transcatheter hepatic arterial embolization with intratumoral dendritic cell infusion for hepatocellular carcinoma: clinical safety. *Clin Exp Immunol* 2007;147: 296–305.
8. Ayaru L, Pereira SP, Alisa A, Pathan AA, Williams R, Davidson B, Burroughs AK, Meyer T, Behboudi S. Unmasking of alpha-fetoprotein-specific CD4(+) T cell responses in hepatocellular carcinoma patients undergoing embolization. *J Immunol* 2007;178:1914–22.

9. Zerbini A, Pilli M, Penna A, Pelosi G, Schianchi C, Molinari A, Schivazappa S, Zibera C, Fagnoni FF, Ferrari C, Missale G. Radiofrequency thermal ablation of hepatocellular carcinoma liver nodules can activate and enhance tumor-specific T-cell responses. *Cancer Res* 2006;66:1139–46.
10. Mizukoshi E, Nakamoto Y, Tsuji H, Yamashita T, Kaneko S. Identification of alpha-fetoprotein-derived peptides recognized by cytotoxic T lymphocytes in HLA-A24+ patients with hepatocellular carcinoma. *Int J Cancer* 2006;118: 1194–204.
11. Gollnick SO, Evans SS, Baumann H, Owczarczak B, Maier P, Vaughan L, Wang WC, Unger E, Henderson BW. Role of cytokines in photodynamic therapy-induced local and systemic inflammation. *Br J Cancer* 2003;88:1772–9.
12. Gollnick SO, Owczarczak B, Maier P. Photodynamic therapy and anti-tumor immunity. *Lasers Surg Med* 2006;38: 509–15.
13. Yamamoto N, Homma S, Sery TW, Donoso LA, Hoober JK. Photodynamic immunopotentiation: in vitro activation of macrophages by treatment of mouse peritoneal cells with haematoporphyrin derivative and light. *Eur J Cancer* 1991;27: 467–71.
14. den Brok MH, Sutmuller RP, van der Voort R, Bennink EJ, Figdor CG, Ruers TJ, Adema GJ. In situ tumor ablation creates an antigen source for the generation of antitumor immunity. *Cancer Res* 2004;64: 4024–9.
15. Kotera Y, Shimizu K, Mule JJ. Comparative analysis of necrotic and apoptotic tumor cells as a source of antigen(s) in dendritic cell-based immunization. *Cancer Res* 2001; 61:8105–9.
16. Sauter B, Albert ML, Francisco L, Larsson M, Somersan S, Bhardwaj N. Consequences of cell death: exposure to necrotic tumor cells, but not primary tissue cells or apoptotic cells, induces the maturation of immunostimulatory dendritic cells. *J Exp Med* 2000;191:423–34.
17. Korbelik M, Sun J, Cecic I. Photodynamic therapy-induced cell surface expression and release of heat shock proteins: relevance for tumor response. *Cancer Res* 2005;65: 1018–26.

18. Takayasu K, Arii S, Ikai I, Omata M, Okita K, Ichida T, Matsuyama Y, Nakanuma Y, Kojiro M, Makuuchi M, Yamaoka Y. Prospective cohort study of transarterial chemoembolization for unresectable hepatocellular carcinoma in 8510 patients. *Gastroenterology* 2006;131:461–9.
19. Matsui O, Kadoya M, Yoshikawa J, Gabata T, Arai K, Demachi H, Miyayama S, Takashima T, Unoura M, Kogayashi K. Small hepatocellular carcinoma: treatment with subsegmental transcatheter arterial embolization. *Radiology* 1993;188:79–83.
20. Yamada R, Kishi K, Sonomura T, Tsuda M, Nomura S, Satoh M. Transcatheter arterial embolization in unresectable hepatocellular carcinoma. *Cardiovasc Intervent Radiol* 1990;13:135–9.
21. Pelletier G, Roche A, Ink O, Anciaux ML, Derhy S, Rougier P, Lenoir C, Attali P, Etienne JP. A randomized trial of hepatic arterial chemoembolization in patients with unresectable hepatocellular carcinoma. *J Hepatol* 1990;11:181–4.
22. Groupe d'Etude et de Traitement du Carcinome Hepatocellulaire. A comparison of lipiodol chemoembolization and conservative treatment for unresectable hepatocellular carcinoma. *N Engl J Med* 1995;332:1256–61.
23. Bruix J, Llovet JM, Castells A, Montana X, Bru C, Ayuso MC, Vilana R, Rodes J. Transarterial embolization versus symptomatic treatment in patients with advanced hepatocellular carcinoma: results of a randomized, controlled trial in a single institution. *Hepatology* 1998;27:1578–83.
24. Llovet JM, Real MI, Montana X, Planas R, Coll S, Aponte J, Ayuso C, Sala M, Muchart J, Sola R, Rodes J, Bruix J. Arterial embolisation or chemoembolisation versus symptomatic treatment in patients with unresectable hepatocellular carcinoma: a randomised controlled trial. *Lancet* 2002;359:1734–9.
25. Lo CM, Ngan H, Tso WK, Liu CL, Lam CM, Poon RT, Fan ST, Wong J. Randomized controlled trial of transarterial lipiodol chemoembolization for unresectable hepatocellular carcinoma. *Hepatology* 2002;35:1164–71.
26. Hsu HC, Wei TC, Tsang YM, Wu MZ, Lin YH, Chuang SM. Histologic assessment of resected hepatocellular carcinoma after

transcatheter hepatic arterial embolization. *Cancer* 1986;57:1184–91.

27. Kenji J, Hyodo I, Tanimizu M, Tanada M, Nishikawa Y, Hosokawa Y, Mandai K, Moriwaki S. Total necrosis of hepatocellular carcinoma with a combination therapy of arterial infusion of chemotherapeutic lipiodol and transcatheter arterial embolization: report of 14 cases. *Semin Oncol* 1997;24: S6–71–S6–80.

28. Kobayashi N, Ishii M, Ueno Y, Kisara N, Chida N, Iwasaki T, Toyota T. Co-expression of Bcl-2 protein and vascular endothelial growth factor in hepatocellular carcinomas treated by chemoembolization. *Liver* 1999;19:25–31.

29. Xiao EH, Li JQ, Huang JF. Effects of p53 on apoptosis and proliferation of hepatocellular carcinoma cells treated with transcatheter arterial chemoembolization. *World J Gastroenterol* 2004;10:190–4.

30. Kanai M, Kohda H, Sekiya C, Namiki M. Effects on interleukin 1 alpha and beta production of peripheral blood mononuclear cells from patients with hepatocellular carcinoma after transcatheter arterial embolization. *Gastroenterol Jpn* 1990;25:662.

31. Yamazaki H, Nishimoto N, Oi H, Matsushita M, Ogata A, Shima Y, Inoue T, Tang JT, Yoshizaki K, Kishimoto T, Inoue T. Serum interleukin 6 as a predicator of the therapeutic effect and adverse reactions after transcatheter arterial embolization. *Cytokine* 1995;7:191–5.

32. Itoh Y, Okanoue T, Ohnishi N, Nishioji K, Sakamoto S, Nagao Y, Nakamura H, Kirishima T, Kashima K. Hepatic damage induced by transcatheter arterial chemoembolization elevates serum concentrations of macrophage-colony stimulating factor. *Liver* 1999;19:97–103.

33. Araki T, Itai Y, Furui S, Tasaka A. Dynamic CT densitometry of hepatic tumors. *AJR Am J Roentgenol* 1980;135: 1037–43.

34. Sobin LH, Wittekind C. TNM classification of malignant tumors, 6th edn. New York: Wiley-Liss, 2002. 81.

35. Terayama N, Miyayama S, Tatsu H, Yamamoto T, Toya D, Tanaka N, Mitsui T, Miura S, Fujisawa M, Kifune K, Matsui O, Takashima T. Subsegmental transcatheter arterial embolization for

hepatocellular carcinoma in the caudate lobe. *J Vasc Interv Radiol* 1998;9:501–8.

36. Okamoto H, Shin J, Mion S, Koshimura S, Shimizu R. Studies on the anticancer and streptolysin S-forming abilities of hemolytic streptococci. *Jpn J Microbiol* 1967;11: 323–36.

37. Nakahara S, Tsunoda T, Baba T, Asabe S, Tahara H. Dendritic cells stimulated with a bacterial product, OK-432, efficiently induce cytotoxic T lymphocytes specific to tumor rejection peptide. *Cancer Res* 2003; 63:4112–8.

38. Japan LCSGo. Classification of primary liver cancer. English edn. 2. Tokyo: Kanehara, 1997.

39. Desmet VJ, Gerber M, Hoofnagle JH, Manns M, Scheuer PJ. Classification of chronic hepatitis: diagnosis, grading and staging. *Hepatology* 1994;19:1513–20.

40. Mizukoshi E, Nakamoto Y, Marukawa Y, Arai K, Yamashita T, Tsuji H, Kuzushima K, Takiguchi M, Kaneko S. Cytotoxic T cell responses to human telomerase reverse transcriptase in patients with hepatocellular carcinoma. *Hepatology* 2006;43:1284–94.

41. Mizukoshi E, Honda M, Arai K, Yamashita T, Nakamoto Y, Kaneko S. Expression of multidrug resistance-associated protein 3 and cytotoxic T cell responses in patients with hepatocellular carcinoma. *J Hepatol* 2008;49:946–54.

42. Ikeda-Moore Y, Tomiyama H, Miwa K, Oka S, Iwamoto A, Kaneko Y, Takiguchi M. Identification and characterization of multiple HLA-A24-restricted HIV-1 CTL epitopes: strong epitopes are derived from V regions of HIV-1. *J Immunol* 1997;159: 6242–52.

43. Kuzushima K, Hayashi N, Kimura H, Tsurumi T. Efficient identification of HLA-A*2402-restricted cytomegalovirus-specific CD8(+) T-cell epitopes by a computer algorithm and an enzyme-linked immunospot assay. *Blood* 2001;98:1872–81.

44. Wissniowski TT, Hansler J, Neureiter D, Frieser M, Schaber S, Esslinger B, Voll R, Strobel D, Hahn EG, Schuppan D. Activation of tumor-specific T lymphocytes by radio-frequency ablation of the VX2 hepatoma in rabbits. *Cancer Res* 2003;63: 6496–500.

45. Korbelik M, Krosl G, Krosl J, Dougherty GJ. The role of host lymphoid populations

in the response of mouse EMT6 tumor to photodynamic therapy. *Cancer Res* 1996;56: 5647–52.

46. Udagawa M, Kudo-Saito C, Hasegawa G, Yano K, Yamamoto A, Yaguchi M, Toda M, Azuma I, Iwai T, Kawakami Y. Enhancement of immunologic tumor regression by intratumoral administration of dendritic cells in combination with cryoablative tumor pretreatment and Bacillus Calmette-Guerin cell wall skeleton stimulation. *Clin Cancer Res* 2006;12: 7465–75.

47. Machlenkin A, Goldberger O, Tirosh B, Paz A, Volovitz I, Bar-Haim E, Lee SH, Vadai E, Tzehoval E, Eisenbach L. Combined dendritic cell cryotherapy of tumor induces systemic antimetastatic immunity. *Clin Cancer Res* 2005;11: 4955–61.

48. Ladhams A, Schmidt C, Sing G, Butterworth L, Fielding G, Tesar P, Strong R, Leggett B, Powell L, Maddern G, Ellem K, Cooksley G. Treatment of non-resectable hepatocellular carcinoma with autologous tumor-pulsed dendritic cells. *J Gastroenterol Hepatol* 2002;17: 889–96.

49. Iwashita Y, Tahara K, Goto S, Sasaki A, Kai S, Seike M, Chen CL, Kawano K, Kitano S. A phase I study of autologous dendritic cell-based immunotherapy for patients with unresectable primary liver cancer. *Cancer Immunol Immunother* 2003; 52:155–61.

50. Lee WC, Wang HC, Hung CF, Huang PF, Lia CR, Chen MF. Vaccination of advanced hepatocellular carcinoma patients with tumor lysate-pulsed dendritic cells: a clinical trial. *J Immunother* 2005;28: 496–504.

51. Lee JS, Thorgeirsson SS. Genome-scale profiling of gene expression in hepatocellular carcinoma: classification, survival prediction, and identification of therapeutic targets. *Gastroenterology* 2004; 127:S51–5.

52. Thimme R, Neagu M, Boettler T, Neumann-Haefelin C, Kersting N, Geissler M, Makowiec F, Obermaier R, Hopt UT, Blum HE, Spangenberg HC. Comprehensive analysis of the alpha-fetoprotein-specific CD8+ T cell responses in patients with hepatocellular carcinoma. *Hepatology* 2008;48:1821–33.

Crucial Contribution of Thymic Sirpα+ Conventional Dendritic Cells to Central Tolerance against Blood-Borne Antigens in a CCR2-Dependent Manner

Tomohisa Baba,* Yasunari Nakamoto,[†] and Naofumi Mukaida[1]*

Thymic dendritic cells (DCs) as well as thymic epithelial cells are presumed to be major sentinels in central tolerance by inducing the apoptosis of autoreactive T progenitor cells. The thymic DC population is composed of heterogeneous subsets including CD11c+B220+ plasmacytoid DCs, CD11c+B220−CD8α+ signal regulatory protein α (Sirpα)− and CD11c+B220−CD8α−Sirpα+ conventional DCs (cDCs). However, the distinctive role of each DC subset remains undefined. We show herein that Sirpα+ cDCs, a minor subpopulation, was disseminated in the thymic cortical area with some of them uniquely localized inside perivascular regions and nearby small vessels in the thymus. The Sirpα+ but not Sirpα− cDC subset can selectively capture blood-circulating Ags. Moreover, in CCR2-deficient mice, the thymic Sirpα+ cDC subset, but not other thymic cell components, was moderately decreased especially in the perivascular regions. Concomitantly, these mice exhibited a modest impairment in intrathymic negative selection against blood-borne Ags, with the reduced capacity to uptake blood-borne Ags. Given their intrathymic cortical localization, CD11c+B220−CD8α−Sirpα+ cDCs can have a unique role in the development of central tolerance against circulating peripheral Ags, at least partially in a CCR2-dependent manner. *The Journal of Immunology*, 2009, 183: 3053–3063.

T he thymus is vital for development of T cells. T progenitor cells in the thymus are subjected to positive and negative selection, and survivors become self-MHC-restricted and self-tolerant mature naive T cells. Negative selection induces clonal deletion of potentially pathogenic autoreactive T cells and consequently decreases the risk of the development of autoimmune disorders (1). Thus, negative selection has a major role in central tolerance. Medullary thymic epithelial cells (mTECs)[2] are major inducers of negative selection. mTECs express the *autoimmune regulator (AIRE)* gene, which induces the ectopic expression of a milieu of peripheral tissue-specific Ags in the thymus resulting in the clonal deletion of autoreactive T progenitors with specificity for these Ags (2–4). Another type of thymic APCs, in particularly dendritic cells (DCs), have also been shown to contribute to negative selection (5–7). However, the detailed molecular and cellular mechanisms by which thymic DCs mediate negative selection remain largely unknown.

Thymic DCs are heterogeneous, similar to DCs in peripheral lymphoid organs such as lymph nodes and spleen. In humans and mice, thymic DCs are classified into two distinct subsets, CD11c+B220+ plasmacytoid DCs (pDCs) and CD11c+B220−

conventional DCs (cDCs). cDCs are further divided into CD11c+CD11b−CD8α+Sirpα− and CD11c+CD11b+CD8α−Sirpα+ subsets (8, 9). CD8α+Sirpα− cDCs, the most abundant subset among these three thymic DC subsets, are clustered in the medulla (10, 11). These CD8α+Sirpα− cDCs also express AIRE and can present endogenous self-Ags. In addition, they can cross-present tissue-specific Ags derived from the mTECs for negative selection (12, 13). In contrast, the intrathymic location and functions of another minor cDC, CD11c+CD11b+CD8α−Sirpα+, subset remain unclear, although this subset is presumed to migrate from the bloodstream (8). Proietto et al. (14) demonstrated that Sirpα+ cDCs can induce thymocytes to efficiently differentiate into regulatory T cells in vitro. However, the roles of Sirpα+ cDCs in central tolerance and regulatory T cell generation in vivo and the nature of the target autoantigens of central tolerance remain elusive.

Chemokines and their receptors have essential roles in controlling the homeostatic homing of immune cells including DCs and T cells (15–17). We examined the composition of thymic DC subsets in mice deficient in CCR1, CCR2, CCR5, or CX3CR1, the chemokine receptors which are expressed by DCs (18, 19). We observed that Sirpα+ cDCs, but not Sirpα− cDCs or pDCs, were selectively decreased in the thymus of CCR2-deficient mice, but not in the other chemokine receptor gene-deficient mice. Interestingly, CCR2-deficient mice exhibited a modest impairment in intrathymic negative selection against i.v. injected Ags. Concomitantly, CCR2 deficiency allowed releasing more autoreactive T cells against serum Ags into periphery. These Sirpα+ cDCs migrated from bone marrow to thymus by the way of the peripheral blood and showed a unique intrathymic localization confined to perivascular and cortical areas. Moreover, Sirpα+ cDCs had a greater capacity to uptake blood-borne Ags than Sirpα− cDCs, along with their unique intrathymic localization. Thus, our present study suggests that thymic Sirpα+ cDCs may function as a specialized APC for the development of central tolerance to blood-borne Ags.

Materials and Methods

Mice

Specific pathogen-free 6- to 7-wk-old male BALB/c mice were purchased from Charles River Japan and designated as wild-type (WT) mice. CCR1$^{-/-}$ and CX3CR1$^{-/-}$ mice were provided by Dr. P. M. Murphy (National Institute of Allergy and Infectious Diseases, National Institutes of Health, Bethesda, MD) (20, 21). CCR2$^{-/-}$ (22) and CCR5$^{-/-}$ mice (23) were provided by Dr. W. Kuziel (University of Texas San Antonio, San Antonio, TX) and Dr. Kouji Matsushima (University of Tokyo, Tokyo, Japan), respectively. All chemokine receptor-deficient mice were back-crossed to BALB/c mice for 8–10 generations. DO11.10 mice expressing a transgenic TCR that recognizes the OVA$_{323-339}$ peptide in the context of I-A^d were maintained as heterozygotes. DO11.10 mice were backcrossed to CCR2$^{-/-}$ mice to generate DO11.10/CCR2$^{-/-}$ mice. Genotyping for the CCR2 gene was done by direct PCR from whole blood samples using an Ampdirect Plus kit (Shimadzu) and the specific primers (sense, 5'-CACGAAGTATCCAAGAGCTTG-3' and antisense, 5'-CCCAAGTGAC TACACTTGTTA-3'). The mouse experiments were performed under specific pathogen-free conditions in accordance with the Guidelines for the Care and Use of Laboratory Animals of Kanazawa University.

Antibodies

Rat anti-mouse mAbs used were anti-CD3ε (145-2C11; Miltenyi Biotec), anti-CD4 (RM4-5; BD Pharmingen), anti-CD8 (53-6.7; BD Pharmingen), anti-CD25 (PC61; BD Pharmingen), anti-CD45R/B220 (RA3-6B2; BD Pharmingen), anti-CD172a/Sirpα (P84; BD Pharmingen), anti-DO11.10 clonotypic TCR (KJ1-26; BD Pharmingen), anti-F4/80 (A3-1; Serotec), and anti-Ly51 (6C3; BioLegend). Hamster anti-mouse CD11c (HL-3) and mouse anti-mouse I-A^d (AMS-32.1) mAbs were purchased from BD Pharmingen. Rabbit anti-mouse CCR2 mAb and anti-mouse type IV collagen (Col IV) polyclonal Ab were purchased from Epitomics and LSL, respectively. Goat anti-mouse MCP-2 polyclonal Ab was purchased from Santa Cruz Biotechnology. Isotype-matched control IgGs for each rat and hamster mAbs were purchased from BD Pharmingen. Mouse, rabbit, and goat IgG (Sigma-Aldrich) served as controls.

Cell preparation

Thymus was digested in 0.6 mg/ml collagenase type IV (Sigma-Aldrich) and 25 Kunitz units/ml DNase I (Sigma-Aldrich) in RPMI 1640 (Sigma-Aldrich) at 37°C for 20 min. The low-density cells were further isolated from the resultant single-cell suspensions using Histopaque-1077 reagent (Sigma-Aldrich). PBMCs were isolated from whole blood using Histopaque-1083 reagent (Sigma-Aldrich). Bone marrow cells were washed out with cold RPMI 1640 medium from the femoral and tibial bones.

Flow cytometry (FCM)

The low-density cells from thymus, PBMCs, and bone marrow cells were stained with various combinations of fluorescent dye-conjugated or non-conjugated specific Abs in PBS supplemented with 2 mM EDTA and 3% FBS. For nonconjugated Abs, fluorescent-conjugated secondary Abs were used. After washing in PBS, expression of cell surface molecular markers was analyzed using a FACSCalibur (BD Biosciences) with CellQuest Pro software (BD Biosciences).

Histology and fluorescent immunohistochemistry

Thymic tissues were frozen in OCT compound (Sakura) and 6-μm-thick cryostat sections were stained with H&E. For immunofluorescence analysis, 6-μm-thick cryostat sections were fixed with cold acetone for 3 min and incubated with Protein Block Reagent (DakoCytomation) to block nonspecific binding. Then fluorescent immunostaining was done by the standard method (for details, see the figure legends). After washing with 0.05% Tween 20-PBS, slides were mounted in fluorescent mounting medium (DakoCytomation). Immunofluorescence was detected in a setting that excluded the nonspecific signal of the isotype control using a fluorescence microscope (BX50; Olympus) or confocal laser-scanning microscope (LSM510; Zeiss). DP Controller software (Olympus) and Zen 2007 software (Zeiss) were used for image processing.

RT-PCR

Total RNAs were extracted from tissues using a RNeasy Mini Kit (Qiagen) and then reverse-transcribed using SuperScript III First-Strand Synthesis System (Invitrogen). PCR was done using the cDNAs, 2.5 mM dNTP mix (Takara), TaqDNA polymerase (Takara), and the specific primer sets for the GAPDH gene (sense, 5'-CAC TGA GCA TCT CCC TCA CA-3' and antisense, 5'-TGG GTG CAG CGA ACT TTA TT-3'), CD45 gene (sense,

5'-AAG ACA GAG TGC AAA GGA GAC-3' and antisense, 5'-TGT AGG TGT TTG CCC TGT GAC AAA GAC-3'), keratin 8 gene (sense, 5'-ACG GTG AAC CAG AGC CTG T-3' and antisense, 5'-CTC CAC TTG GTC TCC AGC AT-3'), MCP-1 gene (sense, 5'-CCC ACT CAC CTG CTG CTA CT-3' and antisense, 5'-TCT GGA CCC ATT CCT TCT TG-3'), MCP-2 gene (sense, 5'-CAG TCA CCT GCT GCT TTC AT-3' and antisense, 5'-ATA CCC TGC TTG GTC TGG AA-3'), and MCP-3 gene (sense, 5'-AAA CAA AAG ATC CCC AAG AGG-3' and antisense, 5'-CAC AGA CTT CCA TGC CCT TC-3') for 30 cycles of 95°C for 30 s, 55°C for 30 s, and 72°C for 30 s.

Effects of a peptide Ag on DO11.10 clonotypic thymocytes

DO11.10-transgenic mice with or without CCR2 gene deficiency were administered 200 μg of OVA$_{323-339}$ peptide (ABGENT) in PBS through the tail vein. To induce thymocyte deletion independently of Ag presentation, mice were injected i.p. with 50 μg of anti-CD3ε mAb (24). Two days after injection, thymocytes were collected and stained with the following combinations of Abs: anti-CD4, anti-CD8, and anti-DO11.10 or anti-CD4, anti-CD25, and anti-DO11.10 Abs. To detect apoptotic cells, thymocytes were stained using an Annexin V-FITC Apoptosis Detection Kit (Merck). After being stained, the cells were analyzed by FCM.

Trafficking of bone marrow-derived immature DCs injected into bone marrow

Bone marrow cells were cultured in RPMI 1640 medium supplemented with 10% FBS and mouse GM-CSF (R&D Systems) at a concentration of 20 ng/ml. An equal volume of culture medium of the same content was added at 4 days, and one-half of the medium was replaced with fresh culture medium at 7 days after the plating. Most bone marrow cells were differentiated into immature DCs as judged by morphological appearances at 10 days after the initiation of the culture. The resultant immature DCs were stained with 1 μM 5-chloromethylfluorescein diacetate (CMFDA; Invitrogen) dye and 1 million cells were injected into the tibial bone marrow cavity of each mouse. After the injection, low-density cells were obtained from thymus, lymph nodes, or PBMCs to determine the presence of CMFDA-stained DCs by using FCM.

Localization of the i.v. injected Ags

Alexa Fluor 488-conjugated OVA protein (OVA$_{488}$), Alexa Fluor 647-conjugated OVA protein (OVA$_{647}$) (Invitrogen), or mouse serum IgG (Sigma-Aldrich), which was conjugated with Alexa Fluor 647, using an Alexa Fluor 647 protein labeling kit (Invitrogen), was injected into the tail vein of mice. Thymic low-density cells and PBMCs were isolated at the indicated time points after OVA protein injection and were stained with anti-CD11c and anti-Sirpα Abs. Then the cells were analyzed by FCM. For the localization of the Ag uptake, cryostat sections of frozen thymic tissues were obtained from mice injected with OVA protein and were stained with anti-Sirpα, anti-CD11c, anti-I-A^d, anti-Ly51, or anti-Col IV Abs and were then observed by fluorescence microscope.

In vitro endocytosis assay

Low-density cells were isolated from the thymus and were incubated with 10 μg/ml OVA$_{647}$ in RPMI 1640 at 37°C for 20 min. As a negative control, incubation was conducted on ice. Endocytosis by each thymic DC subset was analyzed by FCM after being stained with anti-CD11c and anti-Sirpα Abs. In some experiments, low-density cells were preincubated with 10 μM cytochalasin D (Cyt D; Sigma-Aldrich), an actin inhibitor (25), 100 mM ammonium chloride (NH$_4$Cl) (Wako), an inhibitor of the clathrin-dependent pathway (26), or 0.5 mg/ml mannan (Sigma-Aldrich) at 37°C for 15 min before incubation with OVA$_{647}$ at 37°C for 20 min in the presence of fresh inhibitors.

Adoptive transfer of bone marrow cells

Bone marrow cells were obtained from WT or CCR2$^{-/-}$ mice and were stained with 2 μM CMFDA dye. Twenty million cells were injected into the tail vein of CCR2$^{-/-}$ mice. OVA$_{647}$ was injected into the tail vein at 2 days after injection. Thymic low-density cells were isolated at 1 h after OVA protein injection, and the presence of donor-derived Sirpα⁺ cDCs and their capability of Ag uptake were analyzed by FCM.

In vivo cell proliferation assay

Spleen mononuclear cells were isolated from WT or CCR2$^{-/-}$ mice and were labeled with 25 μM CFSE using a CellTrace CFSE Cell Proliferation Kit (Invitrogen). Ten million prelabeled cells were injected into the tail vein of WT mice. One day after injection, mice were immunized with total

FIGURE 1. Effects of chemokine receptor deficiency on mouse thymic DC subsets. *A*, Low-density cells were isolated from WT mouse thymus and were stained with PE-conjugated anti-CD11c, allophycocyanin-conjugated anti-B220, and nonconjugated anti-Sirpα mAbs, followed by staining with FITC-conjugated mouse anti-rat IgG1. The CD11c⁺ DC populations were gated to analyze the expression of Sirpα and B220. *B*, Thymic low-density cells were divided into two groups based on their FSC and SSC patterns, which are indicated by elliptic and square gates. Then DC subsets in each region were analyzed. *C*, Low-density cells were isolated from WT, CCR1⁻/⁻, CCR2⁻/⁻, CCR5⁻/⁻, and CX3CR1⁻/⁻ mice. The Sirpα⁻ and Sirpα⁺ subsets in FSC^high SSC^high CD11c^high B220⁻ cDC populations gated with region 1 (R1) were compared among these mice. *D*, The ratio of two DC subsets (blank portion, Sirpα⁻ subset; gray portion, Sirpα⁺ subset) present in thymic cDC population was determined. Data represent the mean of three independent experiments. *E*, The numbers of Sirpα⁺ DCs in the thymus. Data represent mean ± SD from three independent experiments. *, p < 0.01.
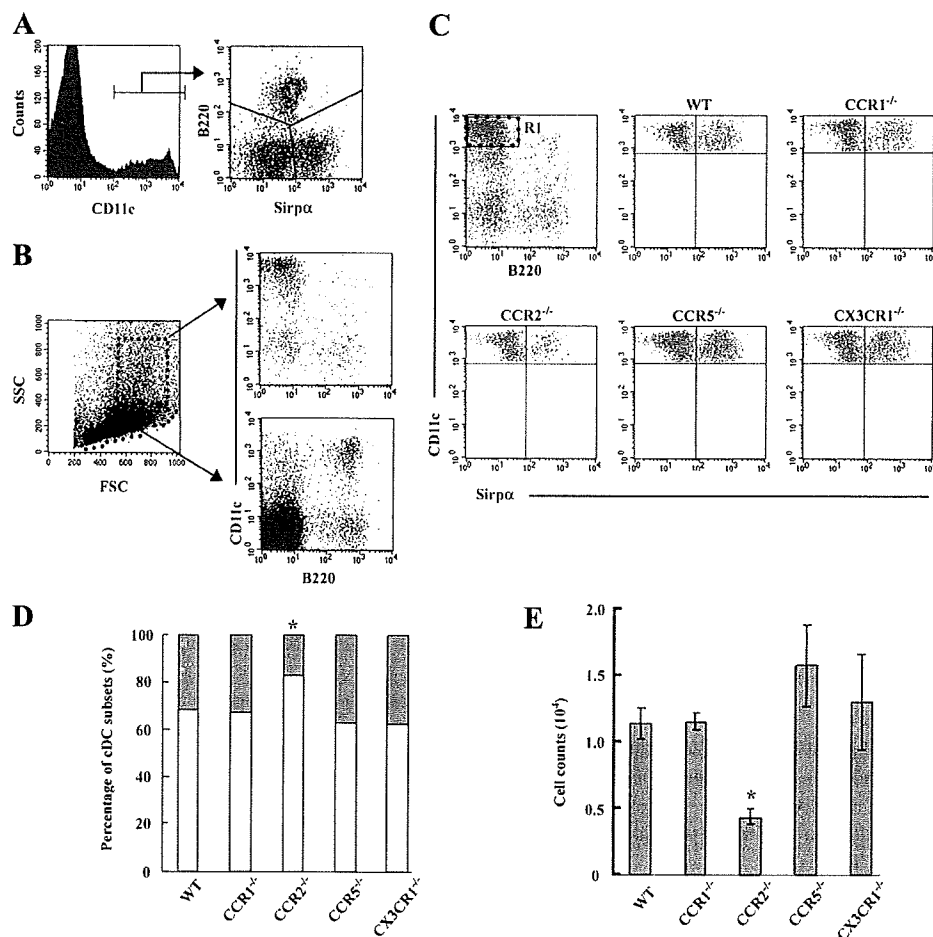
mouse serum protein emulsified in CFA. PBS in CFA was immunized as a control. Two days after immunization, lymphocytes were harvested from draining and nondraining lymph nodes and stained with anti-CD4 mAb. The percentage of CFSE-diluted divided cells was analyzed by FCM.

Statistical analysis

Data are represented as mean ± SD. Statistical significance was determined by one-way ANOVA followed by the Tukey-Kramer test. A value of $p < 0.05$ was considered statistically significant.

Results

Selective reduction of thymic Sirpα⁺ cDCs in CCR2⁻/⁻ mice

Consistent with a previous report (8), three distinct populations of thymic CD11c⁺ DCs have been identified: B220⁺ pDC, B220⁻ Sirpα⁻ cDC, and B220⁻Sirpα⁺ cDC subsets (Fig. 1*A*). cDC and pDC subsets were present mainly in the forward scatter (FSC^high), side scatter SSC^high, and SSC^low areas upon FCM, respectively (Fig. 1*B*). The pivotal role of chemokines in the trafficking of DCs prompted us to examine thymic DC subsets in mice deficient in chemokine receptor genes. Sirpα⁺ DCs were markedly decreased in CCR2⁻/⁻ mice, compared with WT mice, both in the relative (Fig. 1, *C* and *D*) and absolute number (Fig. 1*E*), whereas Sirpα⁻ DC (Fig. 1*C*) and B220⁺ pDC numbers (data not shown) were not changed in CCR2⁻/⁻ mice. In contrast, no significant changes were observed on thymic cDC and pDC subsets in mice deficient in other chemokine receptors including CCR1, CCR5, and CX3CR1. Moreover, we did not observe any differences in thymic B220⁺ B cell and F4/80⁺ macrophage numbers between WT and CCR2⁻/⁻ mice (data not shown). Microscopic studies of the thymus failed to reveal any morphological differences between WT

and CCR2⁻/⁻ mice in terms of the total cellularity, the distribution of thymocytes in each developmental stage, and the localization of Ly51⁺ cortical thymic epithelial cells and I-A^d high mTEC (supplemental Fig. S1³). Thus, CCR2⁻/⁻ mice exhibit a selective decrease in the Sirpα⁺ DC subset in thymus.

Attenuation of OVA₃₂₃₋₃₃₉ peptide-induced clonal deletion by CCR2 gene ablation

Sirpα⁺ DCs are presumed to have the capacity to carry peripheral tissue Ags into the thymus (14). We next investigated the roles of Sirpα⁺ DCs in thymus on taking in an i.v. administered Ag. PBS injection did not cause any changes in each developmental stage of thymocytes in DO11.10 and DO11.10/CCR2⁻/⁻ mice (data not shown). On the contrary, i.v. administration of OVA₃₂₃₋₃₃₉ peptide markedly reduced the proportion and absolute number of clonotypic CD4/CD8 double-positive (DP) thymocytes in DO11.10 mice. CCR2 gene ablation modestly attenuated this reduction (Fig. 2, *A–C*). OVA peptide injection consistently increased the proportion of annexin V⁺ apoptotic cells in DO11.10 mouse thymus compared with that in DO11.10/CCR2⁻/⁻ mice (Fig. 2*D*). In contrast, OVA peptide induced a modest increase in the number of DO11.10⁺CD25⁺CD4⁺ regulatory T cell phenotype to similar extents in both DO11.10 and DO11.10/CCR2⁻/⁻ thymus (Fig. 2*E*). Thus, decreased thymic Sirpα⁺ DCs in CCR2⁻/⁻ mice may be associated with a moderately impaired thymic negative selection. Moreover, following i.p. injection with anti-CD3 Ab (24), thymocytes were deleted to similar extents in DO11.10 and DO11.10/CCR2⁻/⁻ mice

---

³ The online version of this article contains supplemental material.

FIGURE 2. Induction of clonal deletion of DO11.10 clonotypic thymocytes. To induce the clonal deletion, 200 μg of OVA₃₂₃₋₃₃₉ peptide in PBS was injected into the tail vein of DO11.10-transgenic or DO11.10/CCR2⁻/⁻ mice. PBS was injected as a control. DO11.10-transgenic TCR-expressing thymocytes were identified as KJ1-26-positive cells. *A*, Each developmental stage of thymocytes after OVA₃₂₃₋₃₃₉ peptide injection. Percentage of DP stage is shown in each panel. *B*, Percentage of DP stage of development; *C*, the number of DP thymocytes; *D*, percentage of the apoptotic thymocytes; and *E*, the number of CD4⁺CD25⁻ thymocytes were determined on DO11.10 and DO11.10/CCR2⁻/⁻ mice. Representative results from at least four independent experiments are shown in *A* while the mean ± SD was calculated on at least four independent experiments and are shown in *B–E*. *, *p* < 0.05 and **, *p* < 0.01. N.S., No significant difference.
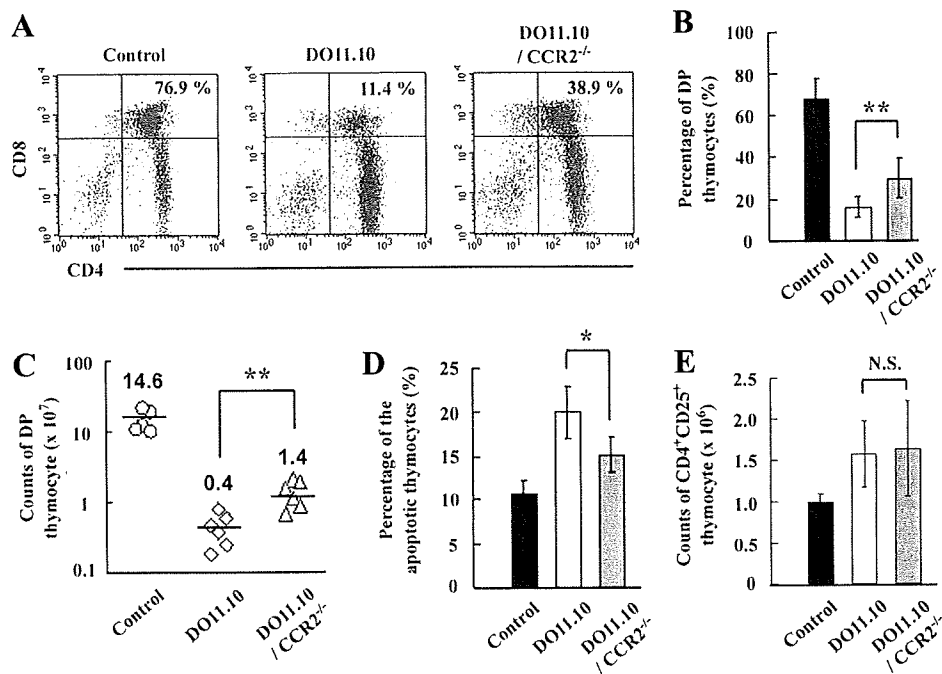
(supplemental Fig. S2), indicating the absence of intrinsic defects of thymocytes in the absence of CCR2. These results collectively suggest that thymic Sirpα⁺ DCs can contribute to intrathymic negative selection of a bloodstream-derived Ag without inducing regulatory T cells.

Thymic Sirpα⁺ DCs can efficiently capture peripheral Ag from bloodstream

To elucidate the functions of thymic Sirpα⁺ DCs more in detail, we determined their intrathymic localization. In thymi of WT mice, Sirpα was mainly detected on CD11c⁺ DCs scattered in the thymic cortex (Fig. 3, *A* and *B*), but not on CD11c⁺ DCs clustered in medulla, the predominating site of thymic CD8α⁺Sirpα⁻ DCs. Moreover, most Sirpα⁺ DCs were localized in close proximity to small vessels with single Col IV⁺ basement membrane or inside perivascular regions (PVRs) separated by two Col IV⁺ basement membranes in the cortex (Fig. 3*C*). The thymic DC population includes APCs crucially involved in the central tolerance system involving bloodstream C5 Ag (27). Furthermore, Sirpα⁺ DCs are selectively localized in PVRs or in close proximity to small vessels, both essential components of the blood-thymus barrier (28). Hence, we hypothesized that this DC subset might be involved in Ag uptake from the bloodstream. To address this possibility, we treated WT mice i.v. with OVA₆₄₇ and examined its uptake by thymic DCs. Intrathymic Sirpα⁺ DCs, but not Sirpα⁻ DCs, took up OVA protein in a dose-dependent manner (Fig. 4*A*), maintaining a stable level from 1 to 4 h after the injection and decreasing thereafter (Fig. 4*B*). Recently, it was reported that bloodstream DCs could efficiently capture and transport particulate bacteria into the spleen when particulate bacteria were i.v. injected (29). Indeed, bloodstream CD11c⁺ cells rapidly disappeared from the peripheral blood after capturing OVA protein (Fig. 4*C*). By contrast, the uptake by intrathymic Sirpα⁺ DCs reached a peak level at 15 min, decreasing to the stable level thereafter. Thus, there may be a remote possibility that circulating DCs migrated into the thymus after capturing OVA protein inside the bloodstream. Furthermore, in addition to an exogenous protein, intrathymic Sirpα⁺ DCs also captured an endogenous serum protein, mouse IgG, which was

conjugated with Alexa Fluor 647, when it was administered i.v. (supplemental Fig. S3). Thus, Sirpα⁺ DCs can effectively capture peripheral Ags from the bloodstream across the blood-thymus barrier. This notion was further supported by the observation that Sirpα⁺ DCs engulfed OVA protein with a higher efficiency than Sirpα⁻ DCs when cultured in vitro with OVA₆₄₇ (Fig. 4, *D* and *E*). Mannan from *Saccharomyces cerevisiae*, but not NH₄Cl or Cyt D from *Zygosporium mansonii*, markedly inhibited endocytosis of OVA protein by Sirpα⁻ DCs (Fig. 4*F*, *upper panel*). On the contrary, uptake of OVA protein by Sirpα⁺ DCs was markedly attenuated by NH₄Cl and Cyt D, but not mannan (Fig. 4*F*, *lower panel*). These observations suggest that thymic Sirpα⁺ DCs can endocytose soluble Ags more efficiently than Sirpα⁻ DCs, in a clathrin-dependent, but not mannose receptor-dependent manner.

Thymic Sirpα⁺ DCs capture peripheral Ag inside PVRs or nearby small vessels, and then migrate into the cortical parenchyma

We examined sequentially intrathymic localization of OVA-derived signals after i.v. injection of OVA₄₈₈. By 0.5 h, OVA₄₈₈-derived signals were detected in Sirpα⁺ cells (Fig. 5*A*), CD11c⁺ DCs (Fig. 5*B*) and inside PVRs or in close proximity to small vessels (Fig. 5*C*). Although some signals remained nearby in small vessels, signals inside PVRs were obviously decreased at 6 h (Fig. 5*D*), as judged by the Col IV immunostaining pattern. At 18 h after the injection, OVA₄₈₈-derived signals were mainly scattered in the Ly51⁺ cortical area but not in the I-Aᵈ ʰⁱᵍʰ medullary area (Fig. 5*E*). Because OVA₄₈₈-derived signals were constantly detected in Sirpα⁺ DCs at every time point (data not shown), these observations suggest that Sirpα⁺ DCs initially capture bloodstream OVA protein inside PVRs or in nearby small vessels and then migrate into the cortical parenchyma. To examine the process of migration more in detail, OVA₆₄₇ (blue) and OVA₄₈₈ (green) were i.v. injected sequentially with an interval of either 6 or 18 h as shown in Fig. 5*F*. When OVA₄₈₈ was injected 6 h after OVA₆₄₇, double-positive CD11cʰⁱᵍʰ DCs were evidently detected (8.1%), while single-positive cells were sparse (Fig. 5*F*, *left upper panel*). Even at 18 h after the injection, double-positive CD11cʰⁱᵍʰ DCs were still

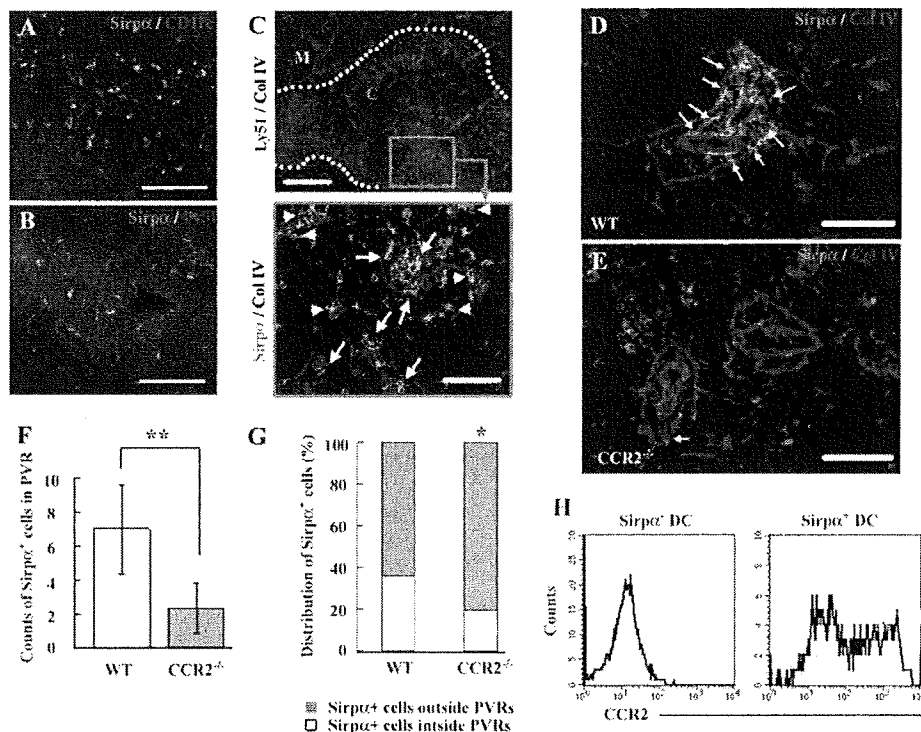**FIGURE 3.** Localization of thymic Sirpα⁺ DCs. Double-color fluorescence immunostaining for Sirpα (green) and CD11c (red; *A*), Ly51 (red; *B*), or Col IV (red; *D* and *E*). *C*, Triple-color fluorescent immunostaining for Sirpα (green), Ly51 (red), and Col IV (blue). Low magnification image for Ly51 and Col IV is shown in the *upper panel*. A green square in the *upper panel* is observed at a higher magnification for Col IV and Sirpα expression and is shown in the *lower panel*. Dashed lines indicate the boundary between cortex (C) and medulla (M). Arrowheads in *C* and arrows in *C–E* indicate Sirpα⁺ cells interacting with small vessels and inside the PVRs, respectively. *A–D*, WT thymus. *E*, CCR2⁻/⁻ thymus. Representative results from at least two independent experiments are shown here. Scale bars: *A* and *B*, 100 μm; *upper panel* of *C*, 200 μm; *lower panel* of *C–E*, 50 μm. *F* and *G*, At least five photographs in the central regions of the PVRs were taken at ×200 magnification in each tissue sample. The numbers of Sirpα⁺ cells inside the PVRs were determined and data represent mean ± SD of three independent experiments. **, *p* < 0.01. *F*, The proportion of Sirpα⁺ cells inside the PVRs to outside was calculated and data represent the mean of three independent experiments. *, *p* < 0.05 (*G*). *H*, CCR2 expression on CD11c^high^Sirpα⁻ or Sirpα⁺ cDCs. Gray-filled and black-open histograms indicate the results from isotype control and specific mAb for CCR2, respectively. Representative results from three independent experiments are shown here.

present (3.2%) with substantial numbers of OVA₄₈₈-derived signal single-positive (3.9%) or OVA₆₄₇-derived signal single-positive cells (2.3%; Fig. 5*F*, *left lower panel*). Thus, CD11c^high^ DCs with Sirpα expression can persistently be in close interaction with the bloodstream while they are migrating into cortical parenchyma (Fig. 5*G*).

Depressed migration of Sirpα⁺ DCs and their aberrant intrathymic localization in CCR2⁻/⁻ mice

It is possible that a decreased intrathymic Sirpα⁺ DC number may account for the defect in their migration in CCR2⁻/⁻ mice, because the thymic Sirpα⁺ cDC subset is presumed to migrate from the bloodstream (14). Most CD11c⁺B220⁻ DCs in peripheral blood and bone marrow expressed abundantly Sirpα (supplemental Fig. S4), similarly as observed on thymic Sirpα⁺ DCs, and this population expressed CCR2 (supplemental Fig. S5). CCR2⁻/⁻ mice exhibited a moderate reduction in CD11c⁺B220⁻ DCs in peripheral blood, but not bone marrow (Fig. 6, *A* and *B*). This suggests a possible defect in the migration of CD11c⁺B220⁻ DCs from bone marrow in CCR2⁻/⁻ mice. To test this possibility, bone marrow cells were induced to differentiate to DCs with in vitro GM-CSF stimulation, labeled with CMFDA, and injected into bone marrow of WT mice (Fig. 6*C*, *upper illustration*). Under these conditions, >80% of injected cells expressed CD11c, Sirpα, and CCR2, but not B220 (supplemental Figs. S4 and S5). WT-derived DCs appeared in peripheral blood rapidly within 2 h after

the intra-bone marrow injection, whereas CCR2⁻/⁻ mouse-derived DCs migrated into peripheral blood less efficiently (Fig. 6, *C* and *D*). Interestingly, CD11c⁺B220⁻Sirpα⁺ DCs appeared in thymus by 6 h after intra-bone marrow injection (Fig. 6*E*). These observations suggest that CCR2-mediated signals were critical of the migration of Sirpα⁺ DCs from bone marrow into the thymus. Moreover, Sirpα⁺ DCs were markedly decreased in PVRs of CCR2⁻/⁻ thymus compared with those of WT thymus (WT mice, 7.0 ± 2.6/site; CCR2⁻/⁻ mice, 2.3 ± 1.5/site; Fig. 3, *D–F*). Furthermore, the decrease was more evident in the region inside the PVRs compared with that outside the PVRs (Fig. 3*G*). CCR2 was expressed also by a portion of intrathymic Sirpα⁻ DCs, but not Sirpα⁻ DCs (Fig. 3*H*). Three mouse chemokines, MCP-1, MCP-2, and MCP-3, can bind to CCR2 (30). Among these chemokines, only MCP-2 mRNA was constitutively expressed in thymus, particularly keratin 8-positive thymic stroma, but not CD45-positive thymocytes (Fig. 7, *A* and *B*). Moreover, MCP-2 immunoreactivities were consistently detected inside the PVRs (Fig. 7*C*, *upper panels*) and on Sirpα⁺ cells in the PVRs (Fig. 7*C*, *lower panels*). Thus, it is probable that the CCR2-MCP-2 interaction can contribute to intrathymic localization of Sirpα⁺ DCs, particularly in the PVRs.

Defective Ag uptake by Sirpα⁺ DCs in CCR2⁻/⁻ mice

Because the PVR was proved to be a main location of the uptake of circulating Ags, we further examined the effects of CCR2
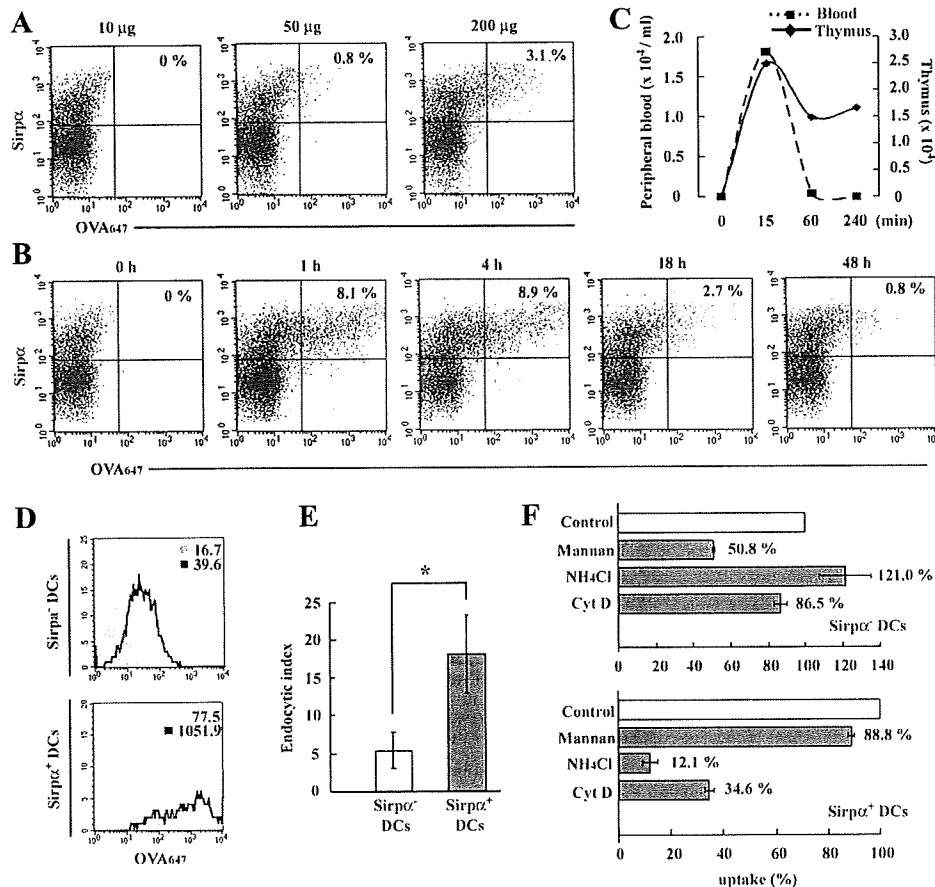
FIGURE 4. Uptake of bloodstream Ag by thymic Sirpα⁺ DCs. A, At 18 h after injection with OVA₆₄₇ at the indicated doses, low-density cells were isolated from WT thymus and were stained with anti-CD11c and anti-Sirpα mAbs. Then the uptake of OVA₆₄₇ in the CD11cʰⁱᵍʰ DC population was analyzed. B, Uptake of OVA₆₄₇ at the indicated time points. OVA₆₄₇ (200 μg) was injected into the tail vein. Percentage of Sirpα⁺OVA₆₄₇⁺ region is shown in each panel of A and B. Representative results from three independent experiments are shown. C, Time kinetics of the numbers of DCs capturing OVA protein in the peripheral blood (broken line) and thymus (solid line). D, In vitro endocytosis of OVA₆₄₇ by CD11cʰⁱᵍʰSirpα⁻ and CD11cʰⁱᵍʰSirpα⁺ cDCs are shown in the *upper* and *lower panels*, respectively. Gray-filled and black-open histograms indicate the results obtained when the cells were incubated at 0 and 37°C, respectively. Numbers in each panel indicates mean fluorescence intensity for OVA₆₄₇ captured. Representative results from three independent experiments are shown here. E, Endocytic index in Sirpα⁻ and Sirpα⁺ cDCs. Endocytic index was calculated as mean fluorescence intensity at 37°C/mean fluorescence intensity at 0°C. Mean ± SD were calculated from three independent experiments and are shown here. *, p < 0.01. F, The effects of various agents on endocytosis. Uptake in the presence of each inhibitor is shown as the percentage of total uptake in the absence of any inhibitors. Means were calculated from three independent experiments and are shown here.

deficiency on the capability of Sirpα⁺ DCs to uptake Ags from the bloodstream. Indeed, when OVA₆₄₇ was injected i.v., CCR2⁻/⁻ mice exhibited a reduced proportion of intrathymic DCs capturing OVA protein compared with WT mice (Fig. 8, A and B). Moreover, after the OVA₆₄₇ injection, Sirpα⁺ DCs of WT mice contained a substantial proportion of OVAʰⁱᵍʰ cells, which represent the cells with a higher uptake of OVA protein, and this population was markedly reduced in CCR2⁻/⁻ mice (Fig. 8, C and D). Moreover, among Sirpα⁺ DCs, the CCR2-expressing population was a main cell type which captured OVA protein (Fig. 8E). CMFDA-labeled WT mouse-derived bone marrow cells appeared in thymus 2 days after the adoptive transfer to CCR2-deficient mice and a substantial proportion of these stained cells expressed CD11c and Sirpα simultaneously (Fig. 8F). Sirpα⁺CD11c⁺ DCs appeared in thymus similarly when CMFDA-labeled CCR2-deficient mouse-derived bone marrow cells were adoptively transferred (data not shown). When OVA₆₄₇ was injected i.v. 2 days after the adoptive transfer, WT donor-derived Sirpα⁺CD11c⁺ DCs captured OVA protein more efficiently than CCR2-deficient DCs in the CCR2-deficient thymus (Fig. 8G). Thus, CCR2-mediated signals may at

least partially regulate the function of Sirpα⁺ DCs to uptake Ag from the bloodstream (supplemental Fig. S6).

Accumulation of autoreactive T cells against serum Ags in the periphery of CCR2⁻/⁻ mice

We observed that CCR2⁻/⁻ mice did not exhibit any signs suggestive of autoimmune disorders until 1 year after the birth (our unpublished data). Hence, we examined whether autoreactive T cells against certain self-Ags in the bloodstream accumulated in the periphery of CCR2⁻/⁻ mice. We examined the accumulation of autoreactive T cells in the draining lymph nodes in WT mice that received CFSE-labeled WT or CCR2⁻/⁻ mouse-derived splenocytes and were subsequently immunized with mouse serum emulsified in CFA. Immunization with total serum protein increased the cell division of CCR2⁻/⁻ mouse-derived CD4⁺ T cells inside draining lymph nodes (10.6%) to a greater extent than immunization with PBS (4.3%; Fig. 9A). Moreover, CD4⁺ T cell division was significantly increased in the recipients of CCR2⁻/⁻ mouse-derived splenocytes compared with the recipients of WT mouse-derived splenocytes (Fig. 9B). Thus, the lack of CCR2 can